เสถียรภาพของโครงสร้างโฮสต์-เกสต์แบบซับซ้อนและตัวนำยวดยิ่งในโลหะแอลคาไล และโลหะแอลคาไลน์เอิร์ทภายใต้ความดันสูง

นายพฤทธิพงษ์ ทรัพยากรเอก

วิทยานิพนธ์นี้เป็นส่วนหนึ่งของการศึกษาตามหลักสูตรปริญญาวิทยาศาสตรดุษฎีบัณฑิต
สาขาวิชาฟิสิกส์ ภาควิชาฟิสิกส์
คณะวิทยาศาสตร์ จุฬาลงกรณ์มหาวิทยาลัย
ปีการศึกษา 2559

STABILITY OF COMPLEX HOST-GUEST STRUCTURE AND SUPERCONDUCTIVITY IN THE ALKALI AND ALKALINE EARTH METALS UNDER HIGH PRESSURE

Mr. Prutthipong Tsuppayakorn-aek

A Dissertation Submitted in Partial Fulfillment of the Requirements
for the Degree of Doctor of Philosophy Program in Physics
Department of Physics
Faculty of Science
Chulalongkorn University
Academic Year 2016

Thesis Title	STABILITY OF COMPLEX HOST-GUEST STRUCTURE AND SUPERCONDUCTIVITY IN THE ALKALI AND ALKALINE EARTH METALS UNDER HIGH PRESSURE
By	Mr. Prutthipong Tsuppayakorn-aek
Field of Study	Physics
Thesis Advisor	Associate Professor Thiti Bovornratanaraks, Ph.D.
Thesis Co-Advisor	Professor Rajeev Ahuja, Ph.D.

Accepted by the Faculty of Science, Chulalongkorn University in Partial Fulfillment of the Requirements for the Doctoral Degree

.....Dean of the Faculty of Science
(Associate Professor Polkit Sangvanich, Ph.D.)

THESIS COMMITTEE

.....Chairman
(Assistant Professor Rattachat Mongkolnavin, Ph.D.)

.....Thesis Advisor
(Associate Professor Thiti Bovornratanaraks, Ph.D.)

.....Thesis Co-Advisor
(Professor Rajeev Ahuja, Ph.D.)

.....Examiner
(Assistant Professor Patcha Chatraphorn, Ph.D.)

.....Examiner
(Assistant Professor Sukkaneste Tungasmita, Ph.D.)

.....External Examiner
(Assistant Professor Pornjuk Srepusharawoot, Ph.D.)

พฤทธิพงษ์ ทรัพยากรเอก : เสถียรภาพของโครงสร้างโฮสต์-เกสต์แบบซับซ้อนและตัวนำยวดยิ่งในโลหะแอลคาไลและโลหะแอลคาไลน์เอิร์ทภายใต้ความดันสูง (STABILITY OF COMPLEX HOST-GUEST STRUCTURE AND SUPERCONDUCTIVITY IN THE ALKALI AND ALKALINE EARTH METALS UNDER HIGH PRESSURE) อ.ที่ปรึกษาวิทยานิพนธ์หลัก: รศ. ดร. ธิติ บวรรัตนารักษ์, อ.ที่ปรึกษาวิทยานิพนธ์ร่วม: ศ. ดร. ราจีฟ อาฮูยา, 72 หน้า.

วิทยานิพนธ์ฉบับนี้ทำการศึกษาเสถียรภาพของโครงสร้างแบบโฮสต์-เกสต์ภายใต้ความดันสูงในธาตุโลหะ แมกนีเซียม ลิเทียม แคลเซียม สแกนเดียมและอาร์เซนิกโดยเทคนิคการคำนวณเชิงทฤษฎี จากการศึกษาโดยเทคนิคการค้นหาโครงสร้างแบบสุ่มในแมกนีเซียมพบว่าภายใต้ความดันสูงในธาตุโลหะแมกนีเซียมมีการเปลี่ยนแปลงโครงสร้างไปเป็นโครงสร้าง I4/mmm และโครงสร้าง Pnma ซึ่งได้รับการทำนายว่าเป็นโครงสร้างที่มีสมบัติเป็นโลหะแบบปกติที่ความดันสูงกว่า 160 GPa นอกจากนี้ผลจากการศึกษาโดยเทคนิคการค้นหาโครงสร้างแบบสุ่มในลิเทียมที่ความดันสูงระบุว่ามีโครงสร้างแบบโฮสต์-เกสต์ ที่สามารถอธิบายได้จากการกระจายตัวของอิเล็กตรอนระหว่างอะตอมโฮสต์กับโฮสต์ซึ่งถูกตรวจสอบด้วยฟังชันก์การรวมตัวของอิเล็กตรอน และการรวมตัวอิเล็กตรอนของพันธะ **π** นี้นำไปสู่ความเสถียรภาพของโครงสร้างแบบโฮสต์-เกสต์ สำหรับการศึกษาในธาตุโลหะแคลเซียมพบว่ามีตัวนำยวดยิ่งอุณหภูมิสูงถึง 25.2 K ที่ความดัน 160 GPa โดยตัวนำยวดยิ่งอุณหภูมิของโครงสร้าง Cc นี้สอดคล้องกับการทดลองตัวนำยวดยิ่ง สำหรับธาตุโลหะสแกนเดียมสามารถอธิบายความเสถียรของโครงสร้างโฮสต์-เกสต์ ใน Sc-II ได้ว่าโครงสร้าง $3c_H$ และ $4c_G$ อยู่รวมกันเป็นโครงสร้างโฮสต์-เกสต์และมีสัดส่วน 4/3 ที่ความดัน 70 GPa นอกจากนี้แล้วการคำนวณโดยเทคนิคการค้นหาโครงสร้างแบบสุ่มได้ทำนายโครงสร้าง Sc-III และพบว่าโครงสร้าง $P4_12_12$ ซึ่งสอดคล้องกับการทดลองตัวนำยวดยิ่งเป็นอย่างดี และสุดท้ายในการศึกษาธาตุโลหะอาร์เซนิกพบว่าโครงสร้างแบบบอดีเซ็นเตอร์เตตระโกนอลซึ่งถูกระบุว่ามีเสถียรภาพที่ความดัน 150 GPa จากเทคนิคการค้นหาโครงสร้างแบบสุ่ม โดยมีลำดับการเปลี่ยนแปลงโครงสร้างภายใต้ความดันสูงคือ จากโครงสร้าง ซิมเปิลคิวบิก เปลี่ยนโครงสร้างไปยัง โฮสต์-เกสต์ ที่ความดัน 41 GPa จากนั้นเปลี่ยนโครงสร้างไปเป็น บอดีเซ็นเตอร์เตตระโกนอล ที่ความดัน 81 GPa ฟังก์ชันสเป็กทรัลของโครงสร้าง บอดีเซ็นเตอร์เตตระโกนอล มีค่าสูงกว่าโครงสร้าง บอดีเซ็นเตอร์คิวบิก ผลการคำนวณพบว่ามีตัวนำยวดยิ่งอุณหภูมิสูงถึง 4.2 K ที่ความดัน 150 GPa

ภาควิชา ฟิสิกส์	ลายมือชื่อนิสิต .....
สาขาวิชา ฟิสิกส์	ลายมือชื่อ อ.ที่ปรึกษาหลัก .....
ปีการศึกษา 2559	ลายมือชื่อ อ.ที่ปรึกษาร่วม .....

5672831023 : MAJOR PHYSICS

KEYWORDS: METAL, HIGH PRESSURE, SUPERCONDUCTIVITY

PRUTTHIPONG TSUPPAYAKORN-AEK: STABILITY OF COMPLEX HOST-GUEST STRUCTURE AND SUPERCONDUCTIVITY IN THE ALKALI AND ALKALINE EARTH METALS UNDER HIGH PRESSURE. ADVISOR: ASSOC. PROF. THITI BOVORNRATANARAKS, Ph.D., CO-ADVISOR: PROF. RAJEEV AHUJA, Ph.D., 72 pp.

This thesis investigates the existence of host-guest structure under high pressure in elemental metals such as Mg, Li, Ca, Sc and As. The new stable structure of magnesium (Mg) is predicted by *ab initio* random structure searching (AIRSS) technique under high pressure. The I4/mmm and Pnma structures have been predicted to give the normal metallic state at the pressure above 160 GPa. Moreover, for Li, the AIRSS technique is used to identify the host-guest (HG) of lithium (Li). The distribution of electrons between the host-host atoms has also been investigated by electron localization function. The strongly localized electron of **π** bond has led to the stability of the HG structure under high pressure. The calculation result from Ca in the metallic phase has led to the discovery of high-T_c superconductivity, with a T_c of 25.2 K at 160 GPa. The T_c of this monoclinic Cc structure is in good agreement with experiment. In addition, the explanation of Sc-II revealed that the $3c_H$ and the $4c_G$ structures coexist which form the HG structure with C_H/C_G ratio of 4/3 at 70 GPa. The AIRSS technique predicts the high pressure structure of Sc-III to be $P4_12_12$ and also reveals T_c of 8.36 K which is in good agreement with the experimental result. Furthermore, the body-centered tetragonal (bct) structure in arsenic (As) has been predicted using AIRSS technique at 150 GPa. The calculation suggests transition sequence from the simple cubic structure transforms to the host-guest structure at 41 GPa and then to the bct structure at 81 GPa. The spectral function of bct structure is higher than those of the bcc structure. This result is also reported to be T_c 4.2 K at 150 GPa.

Department:	Physics	Student's Signature	.....
Field of Study:	Physics	Advisor's Signature	.....
Academic Year:	2016	Co-Advisor's Signature	.....

ACKNOWLEDGEMENTS

It is not easy and possible for me on this thesis accomplished. I would like to thanks all the people who encourage and help me during my studies and research.

I am most grateful to my supervisor Professor Thiti Bovornratanaraks. I would love to express my sincere grateful for letting me do thing my way. I am also very grateful to my second supervisor Professor Rajeev Ahuja, who always encouraged me in my work and who gave me the support I needed and when I am in Uppsala, Sweden.

I would like to thanks to Dr. Wei Luo for always giving a hand if needed and for never avoiding a discussion about our high pressure research when I am in Uppsala, Sweden. I would like to thank Professor Nakorn Phaisangittisakul for answering many questions. I would like to thank Professor Udomsilp Pinsook for advising ab initio molecular dynamics. I would like to thank Dr. Komsilp Kotmool for the help and discussion on Q-ESPRESSO.

Thanks to Pemikar Srifa, Annop Ektarawong, Thawatchart Chulapakorn, Teeraphat Watcharatharapong, Amitava Banerjee, and Emil Edin for a good time at Sweden.

I would like to thanks for supported by research assistant Scholarship from department of chemistry, 90th Year Chulalongkorn Scholarship, and Erasmus Mundus project (EXPERTS SUSTAIN project) for offering scholarships in the academic year 2016/2017.

Last, but not least, I would like to say thank you to my mother, my wife and my family for their encouragement, help, and support.

Finally, I would like to contribute my thesis to my father, who is the inspiration for my life, love dad.

CONTENTS

Page

Page

LIST OF FIGURE

LIST OF ABBREVIATIONS

Å	=	Ångström
β	=	beta
$\alpha^2 F(\omega)$	=	Eliashberg spectral function
C_i^n	=	Coefficient of basis set as *i* in Kohn-Sham orbitals
E_{XC}	=	Exchange-correlation energy
$E_{xc}[n_0(\vec{r})]$	=	Exchange-correlation energy of density functional
ε	=	Eigenvalue
$\varepsilon[n_0(\vec{r})]$	=	Energy: function of density
ε_0	=	Exact ground state energy
$\varepsilon_{xc}[n(\vec{r})]$	=	Exchange-correlation density
$\varphi_j^*(\vec{r})$	=	Complex conjugate
Ψ	=	Kohn-Sham orbital
$\Phi_{\alpha,\alpha'}^{\kappa,\kappa'}$	=	Matrix of force constant
Γ	=	Gamma
γ	=	gamma
H	=	Hamiltonian matrix
k_B	=	Boltzmann constant
λ	=	Electron-phonon coupling
M	=	Mass of nuclei
μ*	=	Effective coulomb interaction
$n(\vec{r})$	=	Density
$n_0(\vec{r})$	=	Electron density: function of positions

$n_0(\vec{r})$	=	Ground state density
O	=	Overlap matrix
Ω	=	Eigenvector
$\omega_{\log}$	=	logarithmic average frequency
ω_m^2	=	Eigenvalue
P	=	Maximum index
π	=	pi
$\vec{R}_I$	=	Atomic position
Θ	=	Debye temperature.
σ	=	sigma
$\vec{u}_{\kappa,\alpha}$	=	Vector of atomic displacements from equilibrium position
$V_{ext}(\vec{r})$	=	External potential
$V_{ee}(\vec{r})$	=	Electron-electron interaction potential
$V_{XC}(\vec{r})$	=	Exchange-correlation potential
AEM	=	Alkaline-earth metals
AIMD	=	*ab intio* molecular dynamics
As	=	Arsenic
AIRSS	=	*ab initio* random structure searching
bcc	=	Body-centered cubic
bct	=	Body-centered tetragonal
BZ	=	Brillouin-zone
Ca	=	Calcium

CASTEP	=	Cambridge Serial Total Energy Package
CALYPSO	=	Crystal structure AnaLYsis by Particle Swarm Optimization
DAC	=	Diamond anvil cell
DFT	=	Density Functional Theory
DOS	=	Densities of states
eV	=	electron Volt
EPC	=	Electron-phonon coupling
ELF	=	Electron localization function
EOS	=	Equation of state
Fcc	=	Face centered cubic
GPa	=	Gigapascal
GGA	=	Generalized gradient approximation
hcp	=	Hexagonal close-packed
HG	=	Host-guest
K	=	Kelvin
LDA	=	Local density approximation
Li	=	Lithium
LMTO	=	Linear-muffin-tin-orbitals
MD	=	Molecular dynamics

MP	=	Monkhorst-Pack
Mg	=	Magnesium
NN	=	Nearest neighbors
NPT	=	Number of atom, Pressure, Temperature
p	=	Any pressure
p_s	=	Search at pressure
PAW	=	Projector augmented wave method
PBE	=	Perdew-Burke-Ernzerhof
PhDOS	=	Phonon density of states
SCF	=	Self-consistent field
Sc	=	Scandium
T	=	Temperature
T_c	=	Superconducting transition temperature
USPP	=	Ultrasoft pseudopotential
USPEX	=	Universal Structure Predictor: Evolutionary Xtallography
VASP	=	Vienna *ab initio* simulation package
V_s	=	Volume of the phase at p_s.
XRD	=	X-ray diffraction
Z	=	Large number of atoms in the unit cell

CHAPTER I
INTRODUCTION

High pressure physics is the important key to understand structural phase transition in elemental metals. One important area of elemental metals within the framework of high-pressure physics finds that there is a fundamental difficulty to get a complete knowledge of crystal structure in elemental metals. The computational physics has been used as a fundamental tool for elemental metals research. Nowadays, it is possible to perform a simulation of elemental metals at the pressure level of the Earth's inner core. Recently, the experiment of high-pressure physics research has exploited diamond anvil cell (DAC) and synchrotron source for investigating materials under the pressure level of the Earth's inner core. Therefore, it is clear that both computational and experimental physics should play a vital role in high pressure research.

With the advent the DAC, one can easily control the pressure for elemental metals of interest in the range of several Gigapascal. In Alkali and alkaline earth metals, they are demonstrated that the structure at ambient pressure transforms into more open structures at high pressure. Interestingly, the complex structure of alkali and alkaline earth finds that they are an incommensurate composite phase consist of two interpenetrating structure. This is due to the fact that two interpenetrating structures are a host and a guest structure which they are the body-centered tetragonal host structure and the face-centered tetragonal guest structure. These two phases are incommensurate along c-axis but they are commensurate in the a-b plane. This type of the incommensurate also has a non-integer number of atoms such as 10.808 atoms of the guest structure of barium (Ba).

However, the simulation of crystal structure relies on the periodicity of the structural model. Therefore, it is not possible to model periodicity of the structure by using only one unit cell. By considering the HG structure, it is described by using supercell along c-axis which approximates the ratio along c-axis. In order to simulate the HG structure, the calculation is performed by using the non-integer ratio of c-axis

of the host structure and c-axis of the guest structure. This ratio is defined as c_H/c_G which also referred as γ.

In the case of Ba, the X-ray diffraction experiment is observed in Ba-IV and obtained the c_H/c_G ratio of 4/3. For simulation of Ba-IV structure, the calculation used the identical ratio of c_H/c_G by approximating the ratio of the $3c_H$ for the host structure and also $4c_G$ for the guest structure.

The relationship between thermodynamically stable structure, electronic structure and superconductivity transition is one of the fundamental questions in high pressure physics. Since the discovery of the HG structure, it superconducting property remained as one of the main questions regarding the very foundation of elemental metals such as magnesium (Mg), lithium (Li), calcium (Ca), scandium (Sc), and arsenic (As). They are fascinating elements in the periodic table for their high-pressure crystal structure as well as their superconducting properties. In this thesis, calculation results are reported along with the stability of HG structure and prediction of superconductivity transition temperature in these elemental metals.

The high-pressure phase in alkali metals under high pressure has been found to be the HG structure such as K-III [1], Rb-IV [2], and Na-IV [3]. Recently, T. Matsuoka *et al.* [4] reported structural phase transitions in Li using experimental apparatus. They reported transition sequence to be Im-3m (0-8 GPa) ⟶F m-3m (8-39 GPa) ⟶ R-3m (39-44 GPa) ⟶ I-43d (44-73 GPa) ⟶ C2mb (73- 80 GPa) ⟶ C2cb (80-120 GPa) ⟶ Cmca (>120 GPa) [5-8]. However, the HG structure was not found among these structures.

Goncharov *et al.* [9] have suggested that Li can be an incommensurate HG structure. Since crystal structure at the pressure above 50 GPa is not known. They suggested the distances between metal atoms in the incommensurate guest chains may be substantially shorter than expected, causing an increase of the phonon frequency because the host modulates the guest atom positions. However, a clear explanation the theoretical aspect has not yet been achieved. Among structural prediction in the crystal structures of materials, Li is one of the most from interested

for structure predictions [10-12] at high pressure. The theoretical study revealed novel structures in Li [10-12] under high pressure but they are no evidence of the HG structure.

The alkaline-earth metals (AEM), which their phase transitions under extreme pressure were suggested to be caused by s-to-d orbital electron transfer from lower pressure to higher pressure phases [13]. The d electrons were suggested to play an important role in describing the electronic structures of AEM. Magnesium (Mg) is one of the AEM, it was calculated in structural energy difference and found that it formed the hexagonal close-packed (hcp) [13]. At high pressure crystal structure of Mg was observed by energy-dispersive X-ray diffraction at room temperature, it transforms into the body-centered cubic (bcc) structure around 5 GPa. [14] The linear-muffin-tin-orbitals (LMTO) calculations predicted a phase-transition sequence from hcp to bcc and to the face centered cubic (fcc) in Mg under increasing pressure [15]. The structural phase transition is not only predicted by the LMTO method but also by a well-known specialized computing code, the Crystal structure AnaLYsis by Particle Swarm Optimization (CALYPSO). The high-pressure crystal structures of Mg have extensively explored by predicting structure at high pressure [16]. They reported that a face-centered cubic (fcc) structure to be stable at 456 GPa. Several AEM has been investigated under high pressure for metallization such as Ca, Sr, and Ba. Especially Ca possesses high-superconductivity temperature of 29 K at 216 GPa [17] and also has the highest T_c among all the metal elements. Moreover, the high-pressure phase of Mg revealed that the fcc structure remains metallic [16]. This suggested that Mg could become superconducting materials under extremely high pressure. Moreover, the existence of the fcc structure has been confirmed to be the stable structure at high pressure but there is no find a crystal structure that it has energetically lower than the fcc structure in the pressure range from 200 - 500 GPa by theoretical study. Recently, the phase diagram of Mg has been investigated by using a combination of x-ray diffraction and both resistive and laser heating [18] at high temperature and high pressure to 211 GPa at 300 K, and to 105 GPa at 4500 K. They also found that the hcp structure transforms to the bcc structure at around 45

GPa. Interestingly, in this study, the high-pressure phase is not reported for Mg beyond the bcc structure and there is no experimental information [18] at low temperature on the high-pressure phases of Mg. This study opens the possibility that at low temperature a new structure may emergence and stable even for pressures above 211 GPa.

Ca is an alkaline-earth metal, which structural phase transition is known to be caused by s-to-d electron transfer [13, 19, 20]. At ambient pressure, the face-centered cubic (fcc) structure, Ca-I, transforms into body-centred cubic (bcc) structure, Ca-II, at pressure 20 GPa and then into simple cubic (sc) structure, Ca-III, at pressure 32 GPa [21, 22]. At pressure above 113 GPa, Ca-III possesses the sc structure and transforms into Ca-IV ($P4_12_12$) at pressure 119 GPa, [23-25] and then into Ca-V (Cmca) at pressure 143 GPa [24, 25] and Ca-VI (Pnma) at pressure 158 GPa [25, 26]. At pressure above 122 GPa, Ca was predicted to be HG structure by *ab initio* calculation. Arapan *et al.* [27] proposed that Ca has a host-guest structure with space group I4/mcm (0,0,γ) which has commensurate value (γ) of 4/3 and it is an isostructural with Sr-V and Ba-IV [28, 29]. Recently, the high-pressure phase at pressure above 210 GPa, Ca-VII was reported to possess the high T_c, with a T_c of 29 K at 216 GPa. Recently, Mao *et al.* [21] reported from experimental study that Ca-III is the rhombohedral structure with spacegroup R-3m. On the other hand, Yao *et al.* [30] suggested that the structure of Ca-III is the sc structure at 300 K by using MD method.

Sc is one of the fascinating transitions metals in the periodic table and continues to attract a lot of attention as it has the HG structure. The HG structure was observed in Sc-II by x-ray diffraction (XRD) experiment [31, 32]. The HG structure in Sc has reported various values of c_H/c_G in channels in along c axis of the host structure. Primarily, the γ of Sc-II was observed by experimental works with the value of 3/2 [31] at lower pressure 23 GPa. On the other hand, at the same pressure, the c_H/c_G of Sc-II phase was identified with the commensurate value of 6/5. [32] They also observed pressure dependence of c_H/c_G. With the increasing pressure, from 23 GPa to 101 GPa the c_H/c_G increased from 6/5 to 4/3 passing through the ideal

commensurate value 4/3 at pressure 72 GPa. In addition, theoretical work by Arapan *et al.* [33] suggested the commensurate value of 14/11 at pressure 17.8 GPa. Therefore, the structural details of HG structure in Sc cannot be concluded both at the low and high pressure which set it apart from other HG structure. With the increasing pressure, Sc-II transforms to Sc-III at pressure 115 GPa. Akahama *et al.* [34] suggested that the structure of Sc-III is a complicated structure with a comparatively large number of atoms in the unit cell (Z). The transitions sequence in Sc is Sc-I (hcp) ⟶ Sc-II (HG) ⟶ Sc-III (unidentified).The Sc-III structure has been observed by XRD which it is stable from 115 to 150 GPa. Unfortunately, the Sc-III structure is not identified yet. [34] The superconductivity of Sc-II phase is the highest T_c. With the increasing pressure, the Sc-II phase is transformed the Sc-III phase. The T_c of Sc-III was observed by experiment [35] and it was reported to possess the T_c, with a T_c of 8.31 K at 111 GPa.

As is one of the group-V elements, the structural phase transition under high pressure is influenced by s-d hybridization from lower pressure to higher pressure phases [36]. At ambient pressure, As possesses a rhombohedral As-type (As-I) structure and transforms into a simple-cubic (As-II) structure at 25 GPa. At higher pressure, it transforms into a body-centered monoclinic host-guest (As-III) structure at 48 GPa, and into a body-centered cubic (As-IV) at 97 GPa. The phase As-IV is stable to at least 122 GPa [37]. For many element metals, [17, 35, 38] with the increasing pressure, it is indicated that the T_c is also increasing. The T_c of As-II (sc) was predicted by Chan *et al.* at 2.99 K and 30 GPa [39]. They also reported that for sc structure T_c decreases monotonically with the increasing pressure at 0.58 K and 50 GPa [39].

As mentioned above, this thesis explores a new structure of Mg by performing the *ab initio* random structure searching (AIRSS) technique [40]. The calculation provided a significant advance in the understanding of the behavior of solid Mg. There have been opened questions for Mg under extreme compression: (i) what is a new structure beyond the bcc structure at high pressure? (ii) Is the metallic high-pressure phase a superconductor? In order to address these problems, the report of theoretical will investigate of the new lowest enthalpy phase of Mg under high

pressure. This research could be greatly helpful for future experiments at low temperature. Moreover, the AIRSS technique is also a powerful theoretical tool for prediction of the stable structure of solid Li. Thus, the AIRSS technique is employed thermodynamics relation in order to predict a new crystal structure of Li under high pressure. In addition, the predicted phase of Ca is proposed the stable structure at above pressure 120 GPa. The calculation is also reported theoretically that it is high-T_c superconductivity. Furthermore, the lack of experimental information of the high-pressure phase of Sc beyond the HG structure, the possibility that a new structure may emergence and stable at above pressure 100 GPa. Since As-IV is stable to at least 122 GPa and there are no reported for the superconductivity in this phase, it would be interesting to investigate the role of electron-phonon coupling (EPC) in order to predict T_c at high pressure. Moreover, there is no high-pressure phase reported from both theoretical and experimental beyond the bcc structure.

CHAPTER II
THEORETICAL BACKGROUND

Density Functional Theory (DFT) is a powerful theoretical tool for calculation of the structural phase transitions. In this study, DFT has been employed in order to investigate structural properties of several metals under high pressure. An early explanation for its most remarkable structural phase transitions is examined by ground state energy. The Kohn-Sham equation is one of the most fascinating high pressure physics which it has model provides to explain of the ground state energy. It can be written as follows:

$$\left[-\frac{1}{2}\nabla^2 + V_{eff}(\vec{r})\right]\Psi_i(\vec{r}) = \varepsilon_i \Psi_i(\vec{r}), \tag{2.1}$$

where the effective potential is

$$V_{eff}[\vec{r}] = V_{ext}(\vec{r}) + V_{ee}(\vec{r}) + V_{XC}(\vec{r}), \tag{2.2}$$

$V_{ext}(\vec{r})$ is the external potential, $V_{ee}(\vec{r})$ is the electron-electron interaction potential, and $V_{XC}(\vec{r})$ is the exchange-correlation potential.

2.1 Born-Oppenheimer Approximation

The Born-Oppenheimer approximation was the first crucial step that possibly made a total energy calculation for a many-body system. We shall start from the full Hamiltonian as following:

$$H = -\sum_{i=1}^{N_e} \frac{\hbar^2}{2m} \nabla_i^2 - \sum_{i,I} \frac{Z_I e^2}{|r_i - R_I|} + \frac{1}{2} \sum_{i \neq j} \frac{e^2}{|r_i - r_j|} - \sum_{I=1}^{N_{nuc}} \frac{\hbar^2}{2M} \nabla_I^2 + \frac{1}{2} \sum_{I \neq J} \frac{Z_I Z_J e^2}{|R_I - R_J|}. \quad (2.3)$$

The five terms on the right hand side of Eq.2.3 are the kinetic energy of electrons, the electron-nuclei interaction, the electron-electron interaction, the kinetic energy of nuclei, and the nuclei-nuclei interaction, respectively. Since mass of the nuclei is much heavier than individual electrons. Thus, the last term of Eq.2.3 can be set to be constant. Therefore, we can obtain a simplified Hamiltonian as shown below:

$$H = -\sum_{i=1}^{N_e} \frac{\hbar^2}{2m} \nabla_i^2 - \sum_{i,I} \frac{Z_I e^2}{|r_i - R_I|} + \frac{1}{2} \sum_{i \neq j} \frac{e^2}{|r_i - r_j|}. \quad (2.4)$$

This is the Born-Oppenheimer approximation, which gives a reasonable energy for a simple system but it is still inappropriate for solving more complicated systems.

2.2 Hohenburg-Kohn Theorem

The starting point for application of DFT to the real system comes from the Hohenburg-Kohn theorem [41] consisting of two theorems as following:

The first theorem states that the ground state expectation value of any observable quantity *H* is a unique functional ground state density. It can be written as:

$$\langle \Psi | H | \Psi \rangle = \varepsilon \left[n_0(\vec{r}) \right], \quad (2.5)$$

$n_0(\vec{r})$ is an electron density: function of positions, and $\varepsilon \left[n_0(\vec{r}) \right]$ is an energy function of density.

The second theorem states that the ground state energy was determined by minimizing total energy, which is a function of electron density, by the vibrational

principle of the energy functional, $\varepsilon\left[n_0(\vec{r})\right]$. This can also be written in the mathematical form, and shown as below:

$$\left.\frac{\delta\varepsilon\left[n(\vec{r})\right]}{\delta n}\right|_{n=n_0} = 0, \tag{2.6}$$

the exact ground state energy, ε_0 corresponding to the ground state density $n_0(\vec{r})$ is given by $\varepsilon_0 = \varepsilon\left[n_0(\vec{r})\right]$.

2.3 Self-consistent Kohn-Sham equation

In condensed matter systems, the exact ground state energy can be solved by the Kohn-Sham equation (Eq. 2.1). Since the systems are complex by their nature, it is extremely difficult to find the ground state energy. Moreover, this equation maps an interacting system to an untrue non-interacting system in which the particles moving in an effective field. Thus, the energy functional in the DFT can be written as

$$\varepsilon\left[n(\vec{r})\right] = T_0\left[n(\vec{r})\right] + \frac{1}{2}\iint d\vec{r}d\vec{r}' \frac{\phi^*_{i\vec{k}}(\vec{r})\phi_{i\vec{k}}\phi^*_{j\vec{q}}(\vec{r})\phi_{j\vec{q}}(\vec{r})}{\left|\vec{r}-\vec{r}'\right|} + \int V_{ext}(\vec{r})n(\vec{r})d\vec{r} + E_{xc}\left[n(\vec{r})\right] \tag{2.7}$$

The right hand side of the total energy equation in Eq. (2.7) consist of four terms, those are non-interacting kinetic energy functional, the electron-electron interacting energy (Hartree energy), the external potential energy due to nuclei and exchange-correlation energy functional, respectively. The total energy obtained by solving the Kohn-Sham equation (Eq.2.1) is in the Hartree unit. The total energy depends on the exchange-correlation energy functional $E_{xc}\left[n_0(\vec{r})\right]$; this term defines the approximate exchange-correlation functional by using only the local density. Therefore, the ground-state energy has been revealed using self-consistent field (SCF) method [42].

In SCF method, the electron density is initially guessed and the effective potential functional is calculated. Then the Kohn-Sham equation is solved in order to get the Kohn-Sham orbitals and the total energies. This procedure is repeated until the electron density is convergent. The entire numerical procedure is described in Fig .1, and Eq. (2.7) can also be called the self-consistent Kohn-Sham equation.

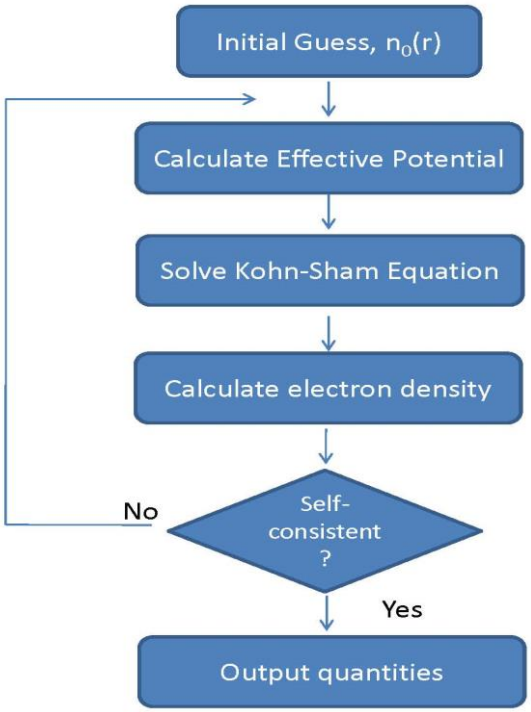

Figure 1. Schematic of the SCF method.

In the process of solving the Kohn-Sham equation using the SCF method, the Kohn-Sham orbitals can be expanded using the basis set:

$$\Psi_n(\vec{r}) = \sum_{i=1}^{P} C_i^n \phi_i(\vec{r}) . \tag{2.8}$$

Where C_i^n is a coefficient of basis set in Kohn-Sham orbitals. Substituting the Kohn-Sham orbitals back into Eq.(2.1), one gets the following equation:

$$\sum_{i=1}^{P} C_i^n [-\frac{\hbar^2}{2m}\nabla^2 + V_{eff}(\vec{r})]\phi_i(\vec{r}) = \varepsilon_i \sum_{i=1}^{P} C_i^n \phi_i(\vec{r}) . \quad (2.9)$$

In Eq. (2.9), the maximum index, *P,* can take any value up to infinity but it has been chosen as large as possible to give the Kohn-Sham orbitals accurately. Multiplying Eq. (2.9) by a complex conjugate $\varphi_j^*(\vec{r})$, and integrating over three-dimension space, one can then obtain an equation shown below:

$$\int d\vec{r} \sum_{i=1}^{P} C_i^n [-\frac{\hbar^2}{2m}\nabla^2 + V_{eff}(\vec{r})]\phi_j^*(\vec{r})\phi_i(\vec{r}) = \varepsilon_i \sum_{i=1}^{P} C_i^n \int d\vec{r}\phi_j^*(\vec{r})\phi_i(\vec{r}) , \quad (2.10)$$

where the left hand side is the Hamiltonian matrix, H, and the right hand side is the overlap matrix, O. Thus, Eq. (2.10) can be written in the matrix form shown below:

$$\mathrm{H}\Omega = \varepsilon \mathrm{O}\Omega , \quad (2.11)$$

where Ω is an eigenvector. Thus, Eq. (2.11) is the *P*x*P* matrix which is used to find eigenvalue, ε. This equation can also be called the "secular equation".

2.4 Local density approximation (LDA) and Generalized gradient approximation (GGA)

As previously mentioned, it is difficult to find the ground state energy. In order to get the ground state energy, the exchange-correlation energy can be solved using the variation method in order to find the exchange-correlation potential. The exchange-correlation energy functional can be written in term of density as below:

$$E_{XC}[n(\vec{r})] = \int \varepsilon_{xc}[n(\vec{r})] n(\vec{r}) d\vec{r} , \quad (2.12)$$

where $\varepsilon_{xc}[n(\vec{r})]$ is the exchange-correlation density that is corresponding to the density $n(\vec{r})$. The existence of exchange-correlation energy functional is guaranteed by the Hohenburg-Kohn theorem, and set from local density approximation (LDA) by Perdew and Zunger [43]. The LDA depends on electron density which describes the homogeneity of the electron gas. In contrast, the generalized gradient approximation (GGA) was initialized by Perdew, Burke, and Ernzerhof [44] for inhomogeneity electron gas. The GGA depends on electron density and gradient of electron density which was described in the condition of the inhomogeneous electron gas. Generally, GGA gives better agreement with experimental data than LDA; however, practically, there are a number of approximate functionals that have been found to yield good results for various physical problems. Finally, GGA has been chosen for our calculation as it includes more realistic physical effects than those of the LDA and more accuracy can be expected. Therefore, ground state energy is given by

$$\varepsilon\left[n(\vec{r})\right] = T_e + V_{ext} + V_H + E_{XC}\,, \tag{2.13}$$

where E_{XC} is the exchange-correlation energy, and can be expressed as

$$E_{XC}\left[n(\vec{r})\right] = \int \varepsilon_{xc}\left[n(\vec{r}), \nabla n(\vec{r})\right] n(\vec{r}) d\vec{r}\,. \tag{2.14}$$

Eq. (2.14) represents exchange-correlation energy functional of the GGA, which depends on electron density and gradient of electron density.

2.5 Molecular dynamics

Before we proceed with the molecular dynamics (MD), it should be worth making a remark that although the DFT is fairly popular and appropriate for solving the ground state energy, it has a limitation. The major flaw comes from the fact that

DFT calculation is performed at 0 K. Therefore, the results obtained from the calculation are based on unrealistic thermodynamic condition. Occasionally, this limitation gives rise to a significant discrepancy between experimental and theoretical reports due to the fact that most experiments are carried out at room temperature. To account for the temperature effect, MD calculation has been developed. Once again, we shall start with the full Hamiltonian as stated in Eq.2.3

Since the full Hamiltonian includes the nuclei terms, the effect of temperature on the motion of nuclei has to be included in order to predict the evolution of the structure under above zero temperature. In order for the nuclei to move, a force must be acting on the nuclei. We can calculate this force from the following equation

$$\vec{F}_I = -\frac{\partial \varepsilon}{\partial \vec{R}_I}. \tag{2.15}$$

Where $\vec{R}_I$ is atomic position. The total energy can be expressed as

$$\varepsilon = \langle \Psi | H | \Psi \rangle. \tag{2.16}$$

Where Ψ represents the Kohn-Sham orbital

$$\begin{aligned}\vec{F}_I &= -\left\langle \Psi \left| \frac{\partial H}{\partial \vec{R}_I} \right| \Psi \right\rangle - \left\langle \frac{\partial \Psi}{\partial \vec{R}_I} \middle| H \middle| \Psi \right\rangle - \left\langle \Psi \middle| H \middle| \frac{\partial \Psi}{\partial \vec{R}_I} \right\rangle \\ &= -\left\langle \Psi \left| \frac{\partial H}{\partial \vec{R}_I} \right| \Psi \right\rangle - \varepsilon \left\langle \frac{\partial \langle \Psi | \Psi \rangle}{\partial \vec{R}_I} \right\rangle \\ &= -\left\langle \Psi \left| \frac{\partial H}{\partial \vec{R}_I} \right| \Psi \right\rangle. \end{aligned} \tag{2.17}$$

This is the Hellmann-Feynman force [45], where wave function can be normalized using ordinary condition, $\langle \Psi | \Psi \rangle = 1$.

MD method can be used to understand and predict the physical properties of solid under temperature. The unified approach of molecular dynamics (MD) and density functional theory (DFT) is proposed by *R. Car* and *M. Parrinello* [46]. In this thesis, finally, DFT calculation combined with MD method through Hellman-Feynman force as shown in Fig.2.

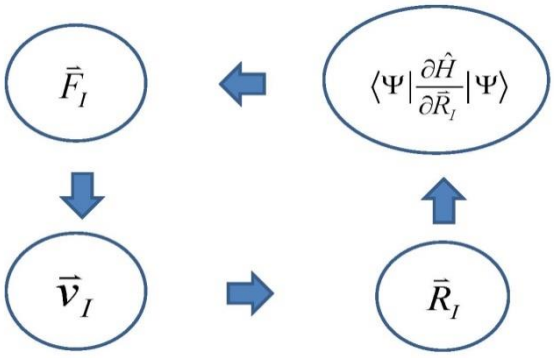

Figure 2. Diagram of Molecular Dynamics (MD) method.

This is a schematic diagram of MD method. First, initial condition was calculated by classical mechanics from the equation of motion or Newton's

equation, $\vec{F}_I = M\vec{a}_I$ where M is a mass of nuclei. The acceleration has to be integrated in order to obtain the velocity which is then integrated again to obtain the position of the nuclei. Next step, we can obtain the force acting on the nuclei through Hellmann-Feynman force. We can equate the temperature with the kinetic energy which can be expressed as

$$\frac{1}{2}mv_I^2 = \frac{3}{2}Nk_BT \ . \tag{2.18}$$

Where k_B is Boltzmann constant. The velocity can be obtained by the Maxwell-Boltzmann distribution. The schematic diagram of MD is not like SCF method in the DFT because the motion of nuclei has been derived depending on the ensemble average.

In order to study the structural phase transition, both DFT and MD have been employed. The two approaches have several differences. Firstly, for the Hamiltonian used in DFT, we used the Born-Oppenheimer approximation as we are interested the electron-electron interaction terms only. On the other hand, for MD, we are interested in the nuclei-nuclei terms as which the forces acting on nucleus can determine explicitly. Moreover, in the MD calculation, electron-electron interaction term was included in the Hamiltonian. The basis set has chosen in the calculation. It is independent of the nucleus position. Secondly, the time considered for both techniques are remarkable different. For DFT, this technique is an important key to the understanding of static properties and it can only be used to calculate the time-independent quantities. In contrast, MD is an important tool to understand the dynamics properties and it can be used to calculate the time-dependent quantities, although, the time in MD composed of two parts which are the real time and the imaginary time. Finally, these two approaches take the temperature effect into account in a very different way. The DFT was considered at T = 0 K in the MD, while the simulation was performed under non-zero temperature.

2.6 *Ab initio* lattice dynamics

In this study, the structural phase transitions under high pressure have been identified based on the DFT calculation at 0 K. Although in several cases, DFT calculations reveal good agreement with the experimental report, it cannot confirm the novel high-pressure phase explicitly. Thus, phonon calculations have also been used to confirm a result from the enthalpy-pressure relation.

First, the expansion has to be performed for the total energy in the structural equilibrium coordinates [47], which is

$$E = E_0 + \sum_{\kappa,\alpha} \frac{\partial E}{\partial \vec{u}_{\kappa,\alpha}} + \frac{1}{2} \sum_{\kappa,\alpha,\kappa',\alpha'} \vec{u}_{\kappa,\alpha} \cdot \Phi^{\kappa,\kappa'}_{\alpha,\alpha'} \cdot \vec{u}_{\kappa',\alpha'} + \ldots \quad . \tag{2.19}$$

These are all zero so the 1st term vanishes and the harmonic approximation the 3rd and higher order terms are assumed to be negligible. Where $\vec{u}_{\kappa,\alpha}$ is the vector of atomic displacements from equilibrium position and $\Phi^{\kappa,\kappa'}_{\alpha,\alpha'}$ is the matrix of force constant $\Phi^{\kappa,\kappa'}_{\alpha,\alpha'} = \dfrac{\partial^2 E}{\partial \vec{u}_{\kappa,\alpha} \partial \vec{u}_{\kappa',\alpha'}}$

At equilibrium, the force acting on these equilibrium atoms can be calculated explicitly, as follows:

$$F_{\kappa,\alpha} = \frac{\partial E}{\partial \vec{u}_{\kappa,\alpha}} \quad . \tag{2.20}$$

Eq. (2.30) was calculated through DFT calculation.

Secondly, plugging this into Newton's equation of motion yields matrix eigenvalue equation, which is:

$$D\varepsilon_m = \omega_m^2 \varepsilon_m \quad . \tag{2.21}$$

Where the dynamical matrix is:

$$D_{\alpha,\alpha'}^{\kappa,\kappa'}(\vec{q}) = \frac{1}{\sqrt{M_\kappa M_{\kappa'}}} \Phi_{\alpha,\alpha'}^{\kappa,\kappa'} . \tag{2.22}$$

The phonon calculation presents the stability of the crystal structure by determining eigenvalue ω_m^2. If phonon of the structure is a positive frequency, the structure is stable. In contrast, if phonon of the structure is a negative frequency, the structure is unstable.

2.7 Superconducting transition temperature

Metallization in many metals has been predicted to give superconducting transition temperature (T_c), which tend to undergo a phase transition to a zero resistivity at low temperature. To find the T_c, the simplest way to achieve the T_c, it can observe $\ln(\Theta/T_c)$ has a linear relation with $(1+\lambda)/\lambda$ in experimental data by McMillan [48] where λ is electron-phonon coupling constant and Θ is the Debye temperature. Consequently, the T_c can be examined with effective Coulomb interaction μ^*. In fact, μ^* is used to fit the formula with experiment. Basically, it contains corrections for repulsive Coulomb interaction in the solid.

Interestingly, McMillan used μ^* = 0.13 for all transition metals and Allen and Dynes assumed μ^* = 0.10 for all metals [49]. The original McMillan formula is correct when λ < 1.4, Allen and Dynes improved it in the case of λ greater than homogeneity.

This is due to the fact that the T_c has been calculated by the Allen–Dynes equation [49]

$$T_c = \frac{\omega_{\log}}{1.2}\exp\left(-\frac{1.04(1+\lambda)}{\lambda-\mu^*(1+0.62\lambda)}\right). \quad (2.23)$$

T_c in terms of the normalized weighting function that arises in Eliashberg theory,

$$g(\omega) \equiv \frac{2}{\lambda\omega}\alpha^2 F(\omega). \quad (2.24)$$

The parameter λ is a dimensionless measure of the strength of $\alpha^2 F(\omega)$

$$\lambda \equiv 2\int_0^\infty \frac{\alpha^2 F(\omega)}{\omega} d\omega, \quad (2.25)$$

and the logarithmic average frequency $\omega_{\log}$

$$\omega_{\log} = \exp\left(\int_0^\infty g(\omega)\ln\omega \, d\omega\right). \quad (2.26)$$

2.8 *Ab initio* random structure searching

High pressure physics is a powerful tool for finding a novel crystal structure of material science such as elemental metals, metal hydrides, metal carbides, and molecular crystal. In order to know the novel crystal structure, it is essential to use the technique for finding and determining symmetry and space group of the crystal structure. By challenging, the methodology was performed by predicting a novel

crystal structure through *ab initio* random structure searching (AIRSS), which is the most popular method for finding an unknown crystal structure.

The AIRSS calculation has already exhibited its capability to examine crystal structures of a broad audience worldwide and that it will play a central and increasing part in materials discovery and design.

The simplest way to generate candidate crystal structure is employed a thermodynamics relation. It is a good idea to get the novel crystal structure through relaxing. Calculations have used the AIRSS technique [50] and *ab initio* calculation of the Cambridge Serial Total Energy Package (CASTEP) [47] to predict a novel crystal structure.

$$H(p) \simeq H(p_s) + (p - p_s)V_s . \tag{2.27}$$

Where p is any pressure and V_s is the volume of the phase at p_s. The quantities $H(p_s)$, p_s and V_s are calculated for each relaxed into higher-symmetry space groups obtained in a search.

Figure 3. The orange circle represents structures and the dashed black arrow local optimization [51].

The AIRSS calculation discovered the idea for finding the global minimum through relaxing. In Fig.3, the orange circle represents structures, the structures find

big basin by relaxing in one-dimension potential energy surface. The AIRSS calculation allows stable structures through the procedure to generate a structure. Particularly, atomic randomly placed in the unit cell and random space group is selected. And then the lattice parameters are randomized, relaxing a reasonable volume to get a specific pressure. Next, a set of sub-group and coordinates are selected randomly to match the number of the atom of metals. After, a k-point grid is generated with a homogeneous density of k-point in each direction. Finally, the crystal structure gets the lowest enthalpy, which is the ground state structure of the system.

CHAPTER III
CALCULATION DETAILS

3.1 Calculation details of magnesium

The calculation of Mg used the AIRSS technique [40] and the CASTEP code [47] to predict the candidate crystal structures under high pressure. The AIRSS approach has been used to predict the crystal structures of materials [12, 40, 52-60]. A plane-wave basis-set with energy cutoff of 240 eV, and an initial Brillouin-zone (BZ) sampling grid of spacing $2\pi \times 0.07$ $A^{\circ -1}$ were used for the calculation. The generalized gradient approximation (GGA) with the Perdew-Burke-Ernzerhof (PBE) parameterization [44] for the exchange-correlation functional to density functional theory was used for the structure searches. The searching calculations are performed using the on-the-fly ultrasoft pseudopotentials [44] as implemented in the CASTEP.

The simulation cells containing 2, 4, 6, 8, and 10 atoms of Mg were calculated at pressures 75, 100, 150, 200, 250, and 300 GPa. The cell shapes and atomic positions are then relaxed to an enthalpy minimum at each pressure. The AIRSS technique generated unit cells of random shapes with reasonable volumes. The AIRSS technique calculated the enthalpies of the phases at any pressure by the simple linear approximation [50].

The calculation is here presented electronic structure by the GGA-PBE [44] for the exchange-correlation functional to density functional theory. The calculation employed the projector augmented wave (PAW) method [61], as implemented in the Vienna *ab initio* simulation package (VASP) [62]. The PAW potential with a 10-electron ($2s^2 2p^6 3s^2$) for Mg has been employed with plane waves up to a cutoff energy of 600 eV and the initial BZ sampling grid of spacing $2\pi \times 0.02$ $A^{\circ -1}$.

All structures were relaxed and their equations of state were obtained by fitting to the calculated energy-volume data to the third-order Birch-Murnaghan equation. Then the calculation was considered the enthalpy-pressure relationship and the high-pressure phase from the experimental information [37].

The dynamical stability of the high-pressure candidate structures were used *ab initio* lattice dynamics with finite displacement method. For the first high-pressure candidate phase (I4/mmm), phonon dispersion was performed by using a supercell 3×3×3. For the second high-pressure candidate phase (Pnma), phonon dispersion was performed by using a supercell 2×2×2. The high-pressure candidate structures were calculated by VASP code combined with the phonopy package [63].

The electron-phonon coupling (EPC) with density functional perturbation theory [64] was calculated the crystal structure of Mg. The plan-wave was expanded with a kinetic energy cutoff of 544.2 eV The calculation studies presented here are based on GGA-PBE as implemented in Quantum Espresso [65]. The BZ integrations in the electronic and phonon calculations were performed using MP meshes. Both the meshes of k-points for electronic states and the meshes of phonons have referred. For the I4/mmm phase, individual phonon calculations were performed on the first BZ on 4×4×4 q-meshes with an 8×8×8 k-points mesh. For Pnma, individual phonon calculations were performed on the first BZ on 2×4×4 q-meshes with a 6×8×8 k-points mesh. For the I4/mmm phase, the EPC matrix elements were computed in the first BZ on 4×4×4 q-meshes using individual EPC matrices obtained with a 16×16×16 k-points meshes. For the Pnma phase, The EPC matrix elements were computed in the first BZ on 2×4×4 q-meshes using individual EPC matrices obtained with a 12×16×16 k-points mesh. This study calculated the T_c by the Allen-Dynes modified McMillan equation [49], which is corresponded for $\lambda < 1.4$.

3.2 Calculation details of lithium

The calculation used the AIRSS technique [40] and *ab initio* calculation of the CASTEP [47] to predict the HG crystal structure of Li under high pressure. The AIRSS approach has been used to predict the crystal structures of materials such as hydrogen [52, 66], helium [67], lithium [12], carbon [68], nitrogen [55, 58, 60], oxygen [59], aluminium [54], strontium [69], metal hydrides [40, 56, 70, 71], and molecular crystals [53, 57, 72]. A plane-wave basis-set energy cutoff of 270 eV, and an initial

Brillouin-zone (BZ) sampling grid of spacing $2\pi \times 0.07$ $Å^{-1}$. The generalized gradient approximation (GGA) with the Perdew-Burke-Ernzerhof (PBE) parameterization [44] for the exchange-correlation functional to density functional theory was used for the structure searches.

Two types of constraint were performed. In the first type, Li atom is placed randomly within the cells and relax cell by shaking. In the second type, Li atom is placed atoms within the cell with crystal symmetry (occupying site 8h of space group I4/mcm) and coordinates x = 0.1486, y = x+0.5, and z = 0 [73] and relax while maintaining the space group symmetry. The cell shapes and atomic positions are then relaxed to an enthalpy minimum at each pressure. We studied simulation cells containing 2, 4, 6, 8, 10, 11, 12, 14, 15 and 24 atoms of Li at pressure 20, 30, 40, 60, 80, 100, and 200 GPa.

The calculation is presented here along with electronic structure calculated at low and high pressures range by the GGA-PBE [44] exchange-correlation functional for the density functional theory. The PAW method [61] was used, as implemented in the VASP code [62]. The PAW potential with a 3-electron (1s2s) for Li has been employed with plane waves basis set up to a cutoff energy of 600 eV and the initial BZ sampling grid of spacing 0.2 Å.

All structures were relaxed and their equations of state were obtained by fitting to the calculated energy-volume data to the third-order Birch-Murnaghan equation. The calculation is determined by the enthalpy-pressure relationship and the high pressure phase from the experimental information [4].

The existence of the HG structure presented here is based on the GGA-PBE using *ab initio* lattice dynamics with finite displacement method as well as supercell scheme by the CASTEP code [47].

3.3 Calculation details of calcium

The AIMD calculation was used for finding a new structure. Because the sc structure is the most stable structure, thus it is used the initial structure. The sc

structure was simulated using supercell consisting of 27 Ca atoms. The sampling of BZ was chosen by MP which was the Γ for sc structure. The MD techniques employed the generalized-gradient approximation (GGA) of Perdew-Burke-Ernzerhof (PBE) [44] exchange-correlation functional. The ultrasoft pseudopotential [75] (USPP) calculation was utilized to treat 3s, 3p, and 4s states as valence states. The plan-wave basis set energy cutoff of 310 eV was used for calculation and it performed the NPT ensemble at 5, 50, and 300 K and 60 GPa which was carried out using 10 fs of integration time step resulting in 5 ps of integrated total time of simulation.

The calculation of Ca used the AIRSS technique [40, 50] with CASTEP code [47] for searching structure. The simulation of Ca performed unconstrained searches 2, 4, 6, 8, and 10 atoms per cell at 40, 60, 80, and 100 GPa and the USPEX method [74] with an interface to the VASP code [61, 62]. The searches were performed by varying cell size 6 and 8 atoms per cell and operated at 60 and 100 GPa. We used the efficient the AIRSS technique and the USPEX method, which have both been successfully applied to investigating structures of Ca at high pressures.

For phase transition determination, DFT calculation was performed by CASTEP code with self-consistence field (SCF) method. [41, 42] Similar to MD method mentioned above, PBE [44] exchange-correlation potential functional was used as a structural optimization method. USPP was also employed to treats 3s, 3p, and 4s states as valence states. For DFT calculation, 600 eV was tested for convergence and consequently employed as plane wave energy cut off. The irreducible Brillouin Zone (BZ) consisted of Monkhorst-Pack k-point sampling [76] of 10×10×10 k-points for fcc, bcc and β-tin structure. On the contrary, host-guest and candidate structure used 2×2×1 and 4×4×4 k-point mesh, respectively. The calculations were based on the primitive cell for the candidate structure and based on the conventional cell for other structures. The enthalpy-pressure curve was fitted by the third order Birch-Murnaghan equation of state (EOS) [77].

The stability of high-pressure phases and phase transition were determined using enthalpy-pressure relation. In order to investigate the stability of the candidate structure, lattice dynamics calculation [47] via finite displacement using CASTEP [47]

were performed at 160 GPa resulting in phonon dispersion. For T_c determination, the EPC was accomplished by density functional perturbation theory [64] via linear response using Quantum Espresso [65]. The plan-wave energy cutoff of 544.2 eV was used in both calculations. To investigate EPC, BZ integrations for MP k-point mesh. EPC matrix elements were computed in the first BZ on 2×2×2 q-meshes using individual EPC matrices obtained with 16×16×16 k-points mesh for the high-pressure phase of the candidate structure.

3.4 Calculation details of scandium

In order to find the lowest total energy of the HG structure, the parameter of c_H/c_G was calculated by approximating with a commensurate supercell in along c axis. The Sc-II phase was found to be aperiodic structure as the component of the guest structure made up of chains that lie in channels in along c axis of the host structure. It is well known that the guest structure is incommensurate with the host structure. To treat the parameter of c_H/c_G, the HG structure has kept the parameter of c_H/c_G in channels in along c axis of the host structure. The stability of the HG structure is expected to be related with the parameter of c_H/c_G. The ideal commensurate value with the parameter of c_H/c_G =4/3=1.333 has been proposed and will be used for this simulation [36]. The HG structure calculation was performed in density functional theory (DFT) using CASTEP code [47]. The Generalized-Gradient-Approximation (GGA) with Perdew-Burke-Ernzerhof (PBE) was used. [44] The ultrasoft pseudopotential [75] treats $3s^2$, $3p^6$, $3d^1$, and $4s^2$ states as valence states for Sc has been performed. The calculation of Sc-II was separated the HG structure to be two structures (the host and the guest structures). The stability of Sc-II was calculated for the value of γ=4/3. All the conditions were performed by optimizing structures under high pressure from 50 to 150 GPa.

The parameter of 4/3 was calculated by AIMD calculation. The NPT ensemble [78] was performed in the AIMD calculation in order to examine the thermodynamics stability with the applying pressure. The calculation was employed the 32-atom at

pressure 72 GPa and temperature 300 K and the calculation was performed at 10 fs of integration time step and 2 ps of integrated total simulation time. In addition, the irreducible Brillouin Zone (BZ) consisted of Monkhorst-Pack k-point sampling [76] of 3×3×2 k-points. The unknown structure of Sc-III is calculated by DFT method and AIRSS technique. This calculation leads to the discovery of Sc-III structure, which it is not verified by experiment. The AIRSS [40, 50] has also performed at pressure 80, 100, and 120 GPa and the simulation cells containing 2, 4, 6, 8, 10 and 12 atoms are used at each pressure. The AIRSS technique is an approach to obtain the local minima structure by giving the lowest enthalpy. The shape is generated by shaking from within a reasonable pressure range. The calculation of unknown structure found three relatively low-enthalpy structures ($P2_1/c$, Cmcm, and $P4_12_12$). A plane-wave basis set energy cutoff 380 eV and the BZ sampling grid of spacing $2\pi \times 0.04$ $Å^{-1}$ were used. The Local-Density Approximation (LDA) [43] exchange-correlation functional is found to be sufficient for the initial structures searching and the ultrasoft pseudopotential [75] treats $3s^2$, $3p^6$, $3d^1$, and $4s^2$ states as valence states. This relaxed structure scheme is repeated by searching many times and also the small system is often successful.

The structural phase transition and stability of Sc was calculated by the DFT calculations with the self-consistent field (SCF) method. [42] The ultrasoft pseudopotential [75] and the GGA with PBE [44] exchange-correlation functional were utilized. A plane-wave basis set energy cutoff of 380 eV found a sufficient for finding the ground state energy. The irreducible BZ consisted of MP k-point sampling [76] of 12×12×6, 2×2×1, and 8×8×12 for Sc-I, Sc-II, and a candidate structure, respectively. The EPC with density functional perturbation theory [64] was calculated by Quantum Espresso. [65] The plan-wave basis set energy cutoff of 816.3 eV. The BZ integrations in the electronic and phonon calculations were performed using MP meshes. Both the meshes of k-points for electronic states and the meshes of phonons have referred. The EPC matrix elements were computed in the first BZ on 2×2×3 q-meshes using individual EPC matrices obtained with a 16×16×24 k-points mesh for

the high-pressure phase of Sc-III. The calculation tested several effective Coulomb interaction parameter μ^{*} = 0.10, 0.13, 0.15, 0.16, and 0.18.

3.5 Calculation details of arsenic

The AIRSS technique [40, 50] and *ab initio* calculation of the CASTEP code [47] were exploited to predict the candidate crystal structures of As under pressure. A plane-wave basis-set energy cutoff of 280 eV and an initial Brillouin-zone (BZ) sampling grid of spacing $2\pi \times 0.07 Å^{-1}$ were used. The GGA-PBE parameterization [44] for the exchange-correlation functional was used for the structure searches. The AIRSS technique generated unit cells of random shapes with reasonable volumes.

The calculation of As studied simulation cells containing 2, 4, 6, 8, 10, and 12 atoms of As at pressure 100, 150, 200, 250, and 300 GPa. The cell shapes and atomic positions are then relaxed to an enthalpy minimum at each pressure. The AIRSS technique calculated the enthalpies of the phases at any pressure by the simple linear approximation [50].

The calculation is here presented electronic structure by the GGA-PBE [44] for the exchange-correlation functional to density functional theory. The calculation of As employed the PAW method, [61] as implemented in the VASP code. [62] The PAW potential with a 15-electron ($3d^{10}4s^{2}4p^{3}$) for As has been employed with plane waves up to a cutoff energy of 500 eV and the initial BZ sampling grid of spacing $2\pi \times 0.02$ Å.

All structures were relaxed and their equations of state were obtained by fitting the calculated energy-volume data to the third-order Birch-Murnaghan equation. The calculation presented the enthalpy-pressure relationship and the high-pressure phase from the experimental information.

The phonon dispersion of candidate structure was calculated by *ab initio* lattice dynamics with finite displacement method, as implemented in VASP code and the phonopy package [63]. The candidate structure was used the EPC with density functional perturbation theory [64]. The plan-wave was expanded with a kinetic energy cutoff of 816.3 eV. The calculation studies presented here are based on GGA-

PBE. The calculation employed PAW method as implemented in Quantum Espresso. [65] The BZ integrations in the electronic and phonon calculations were performed using MP meshes. Both the meshes of k-points for electronic states and the meshes of phonons have referred. For As-IV, individual phonon-phonon calculations were performed on the first BZ on 4×4×4 q-meshes with a 12×12×12 k-points mesh. For high-pressure candidate structure, individual phonon-phonon calculations were performed on the first BZ on 4×4×4 q-meshes with an 8×8×8 k-points meshes. For As-IV, The EPC matrix elements were computed in the first BZ on 4×4×4 q-meshes using individual EPC matrices obtained with a 24×24×24 k-points mesh. For high-pressure phase, The EPC matrix elements were computed in the first BZ on 4×4×4 q-meshes using individual EPC matrices obtained with a 16×16×16 k-points mesh. This study calculated T_c using the approximated the Allen-Dynes equation, which is corresponded for $\lambda < 1.4$.

CHAPTER IV
STRUCTURAL PREDICTION IN ELEMENTAL METALS

In the chapter, calculation results from Mg, Li, Ca, Sc, and As are presented and discussed. The AIRSS technique is used to identify the high-pressure phases. For Mg, the structural prediction is calculated at high pressure. The candidate structure is confirmed as the stable structure by phonon calculation at high pressure. Moreover, the calculation of Li predicts that the host-guest structure is the stable structure. For Ca, The metallization of Ca is predicted by AIMD calculation at low and room temperatures. For Sc, a structural phase transition is calculated up to 200 GPa. Finally, for As, the bcc and body-centered tetragonal (bct) structures are predicted to be thermodynamically stable. The calculation of these metals gives a clear understanding for the interpretation of previous experimental findings.

4.1 Stable normal metallic structure of magnesium under high pressure

The AIRSS technique gives an excellent explanation for low-enthalpy of high-pressure phases [40]. Two particular low enthalpy structures of Mg are found, namely the tetragonal and the orthorhombic structures. The optimization of the tetragonal structure with spacegroup I4/mmm at pressure 160 GPa are a = 2.688 Å, b = 2.688 Å, and c = 2.686 Å with Mg atoms located at 2a symmetry sites (0, 0, 0). Furthermore, the optimization of orthorhombic with spacegroup Pnma at pressure 250 GPa are a = 5.061 Å, b = 5.061 Å, and c = 2.561 Å with Mg atoms located at symmetry sites 4c (0.37495, 0.25, 0.74995).

The experimental study [18] reported that the hcp structure transforms into the bcc structure around 45 GPa and 390 K. In this study, similarly, the calculation reveals that the hcp transforms into the bcc structure at pressure 58 GPa and then it transforms into the I4/mmm structure at the pressure 154 GPa. Finally, the I4/mmm structure transforms into the Pnma structure at pressure 221 GPa by determining enthalpy-pressure relation (Fig 4).

The calculation of Mg is shown that the I4/mmm and Pnma structures are energetically more favorable than the fcc structure. This result should also be noted that the transformation of the bcc structure into the fcc structure can easily occur at high temperature.

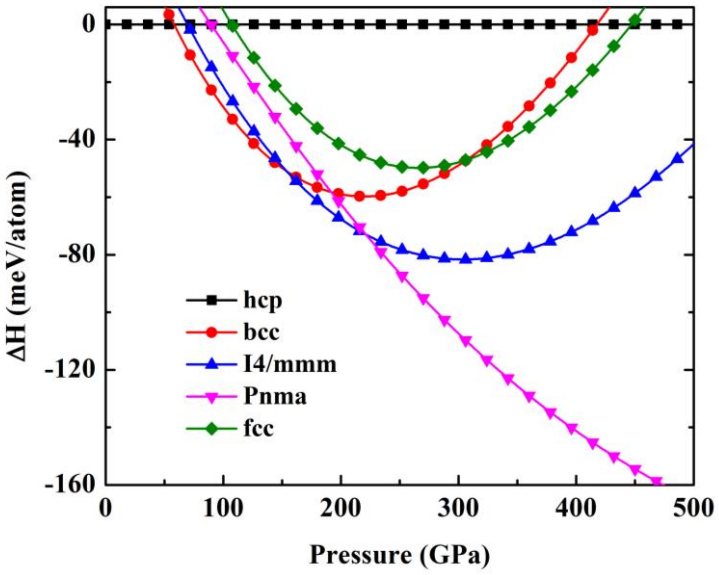

Figure 4. Calculated enthalpies Mg in the pressure range 0-500 GPa. The enthalpies of the hcp structure are taken as the reference.

The dynamic stability of the I4/mmm and Pnma structures are identified by the phonon calculation. Because of the lacking of imaginary frequencies, it provides confirmation that the I4/mmm structure is stable at 160 GPa and the Pnma structure is stable at 250 GPa as can also be seen Fig 5.

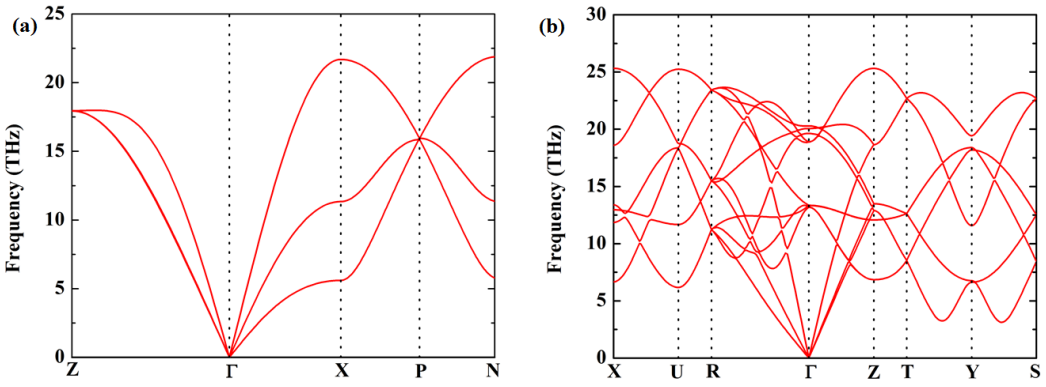

Figure 5. Harmonic phonon dispersion of (a) I4/mmm and (b) Pnma structures calculated at 160 and 250 GPa (T= 0 K), respectively.

4.2 Structural prediction in lithium

The experimental study has observed an unknown phase above 50 GPa [9]. In this study, three interesting structures, I4/mcm, R-3m, and Fd-3m, are proposed by the AIRSS technique. The calculation obtains the lowest-enthalpy crystal structure with spacegroup I4/mcm. To treat the parameter of c_H/c_G, the HG structure keeps the commensurate value in channels in along the c axis of the host structure. The lowest total energy of the HG structure is calculated by approximating with a commensurate supercell along the c axis. This is due to the fact that the HG structure is the aperiodic structure along c axis because the component of the guest structure makes up of chains that lie in this channel of the host structure. Therefore, it is well known that the guest structure is incommensurate with the host structure.

In order to accurately calculate the parameter c_H/c_G of the HG on applied pressure, The stability of the HG structure presents the parameter c_H/c_G through various commensurate analogs with respect to the parameter c_H/c_G = 4/3 = 1.333. By approximating the complex HG structure, γ = 4/3, a commensurate supercell of the host structure is generated $3c_H$ and also the guest structure with $4c_G$. The calculation chooses the following set of the γ values for c_H/c_G: 4/3, 14/11, 5/4, 6/5, 3/2, 5/3, 8/5, and 10/7, which yields two kinds of structure as far as symmetry is involved. The calculation determines by examining total energies of various commensurate analogs with respect to the energy of the parameter c_H/c_G = 4/3 as can be seen in Fig.6. The commensurate of 4/3 is the most energetically stable over a wide range of volumes. The calculation indicates a dramatic increase of the energy difference of the HG structure. At the highest pressure, it shows compressibility of the HG structure that the HG structure with the γ = 4/3 (1.333) transforms into 3/2 (1.5) and it transforms into 8/5 (1.6), respectively.

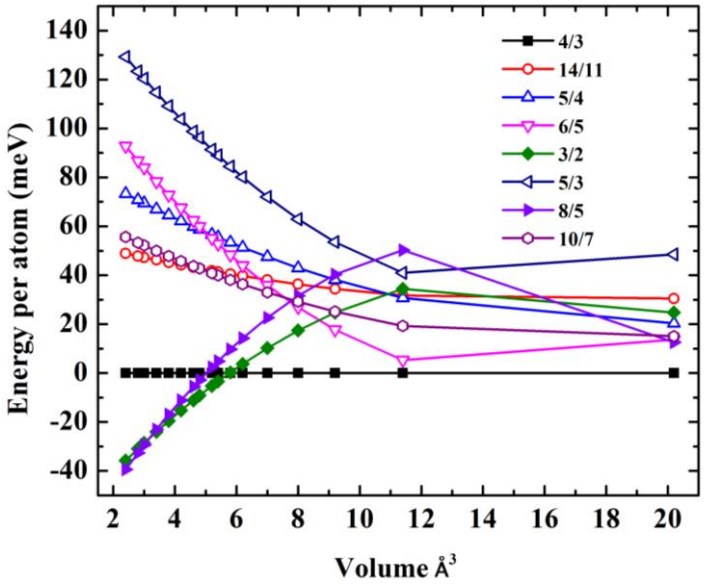

Figure 6. Total energies of various commensurate analogues with respect to the energy of the commensurate supercell with commensurate value γ = 4/3 as a function of volume/atom.

The enthalpies of the more stable phases are calculated at the higher level of accuracy for enthalpies of different Li phases with respect to the I-43d structure (see Fig.7). The calculation of Li precisely indicates that it is thermodynamically stable over a wide range of pressures. At the pressure around 50 GPa, Two phase transition sequences can be obtained as shown below:

Simple : Fm -3m ⟶ C2mb ⟶ C2cb

Complex : I-43d ⟶ R-3m ⟶ I4/mcm

For the transitions sequence at 0 K, the calculation shows that the fcc structure is the most energetically favorable and it transforms into C2mb and then it transforms into C2cb, respectively. It is the simple structural phase transformation. The calculation of Li reveals that the C2mb is stable in a very narrow pressure range. Moreover, first-principle calculations evaluate the complex structural phase transformation at finite temperature by determining enthalpy-pressure (Fig.7). The I-43d structure transforms into the R-3m structure and then it transforms into the I4/mcm structure.

The I4/mcm structure is predicted that it is thermodynamically stable at high pressure. The inset to Fig.5 shows that the I4/mcm structure is energetically more favorable than the fcc structure above 110 GPa. Interestingly, the calculation indicates pressure-induced phase transitions in the fcc structure. This finding suggests that both complex structures (C2mb, C2cb) and the I4/mcm can be found experimentally at 0 K and 300 K, respectively.

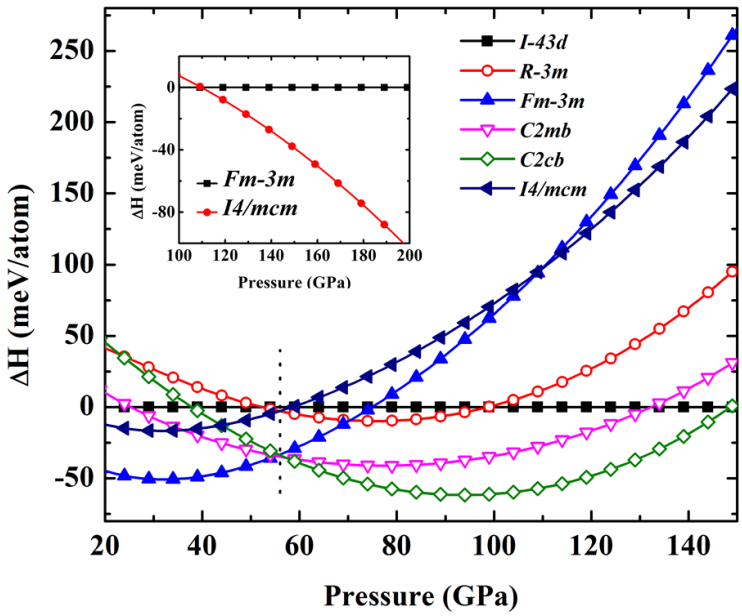

Figure 7. Comparison of the enthalpies of Li phases up to 150 GPa. Li structures relative to the I-43d structure at 0 K. The inset shows the enthalpy of the fcc structure with the I4/mcm.

The HG structure of Li is optimized at pressure 150 GPa. In Fig.8, the HG structure of Li is a commensurate supercell in along c axis by approximating c_H/c_G = 4/3. The optimized structural parameters of the host structure are a = 4.525 Å and c = 2.856 Å with Li atoms located at 8h symmetry sites of spacegroup I4/mcm at (0.166, 0.666, 0) and the guest structure placed atom at (0, 0, 0).

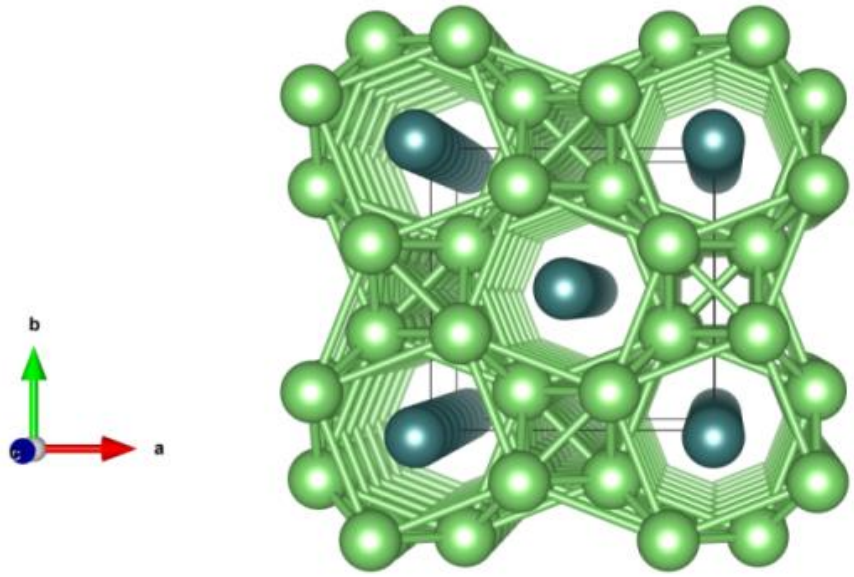

Figure 8. The crystal structure of the host-guest structure of Li. The host structure (dark green atoms) with guest chains (light green atoms) is shown in a c-axis projection.

The distances between the first (host-guest) and second (host-host) nearest neighbors (NN) are 2.927 Å and 4.140 Å at pressure 0 GPa, 2.252 Å and 3.185 Å at pressure 30 GPa, and 1.687 Å and 2.385 Å, at pressure 150 GPa, respectively. Displays a schematic of the HG structure combined with an electron localization function (ELF) as can be seen Fig.9). By comparing the ELF of the HG structure in the (001) planes revealed strongly and weakly in the bonding network at pressures 0, 30, and 150 GPa, respectively. The calculation of Neaton and Ashcroft [80] reported the localization of electron density interstitial regions with "pair" of electrons. The core region the s-pπ hybridization state [80] has led to the localization of electron density. At ambient pressure, it is regularly distributed electrons with s(σ)-p(π) bonding between the host-guest atom and the host-host atom.

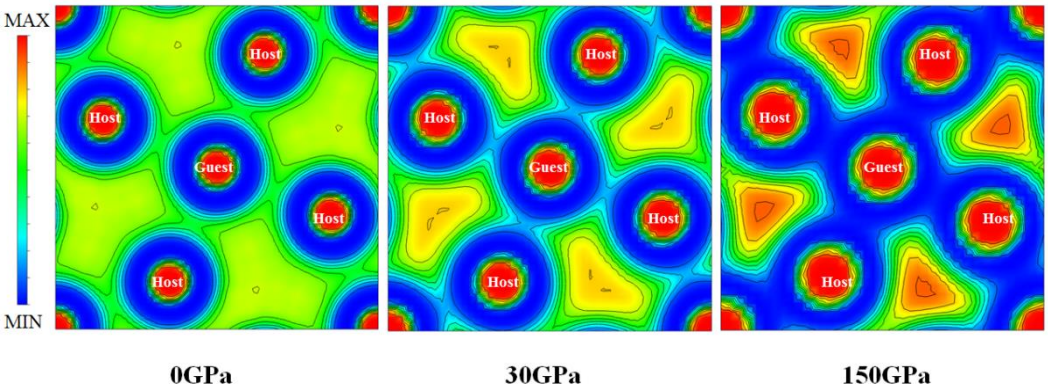

Figure 9. The electron localization function (ELF) in the (001) atomic plane of the host-guest structure of Li under pressures of 0, 30, and 150 GPa.

With the increasing pressure, at 30 GPa, the ELF indicated a slight decrease in the distribution of electrons between the host-guest atom and it indicated σ bond led to the weakly bonding. While the distribution of electrons is increased in between the host-host atom and it is strongly localized electron of π bond. It is obvious that the distribution of electrons becomes rougher at pressure 150 GPa. The accumulation of electrons between host-host atom shows that the bonds are strong bonding in the pπ state. Bonding is favored in π bond when the interatomic distance is shorter than 1.687 Å, which therefore contributes to the stability of the HG structure at high pressure.

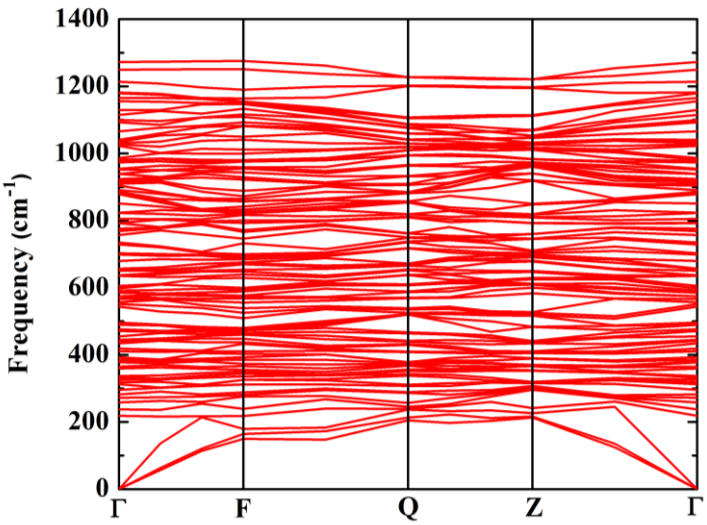

Figure 10. The dynamical harmonic stabilization of the HG structure at pressure 180 GPa.

To investigate the mechanical stability of dense Li, the HG structure is calculated dynamical harmonic stabilization. The dynamical stability is obtained from the phonon dispersion relation as a function of pressure (Fig.10). At pressure180 GPa, the lack of imaginary frequencies provides a good confirmation that the HG structure is stable. This calculation also observed high-frequency band from phonon dispersion which it gives a significant contribution to the strongly localized electron of π bond. Moreover, the distances between the host-host atoms indicated the hardening phonon and it has led to the stabilization of the HG structure.

4.3 Structure prediction of calcium at high temperature and high pressure

The high-pressure phase prediction of Ca obtains three particularly low enthalpies by the AIMD calculation with the sc structure, the Cc structures, and the P1 structure at pressure 60 GPa and at temperatures 300, 50, and 5 K, respectively as shown in Fig.11. Interestingly, the sc structure transforms into the monoclinic structure with space group Cc at 50 K and 60 GPa. This monoclinic complex structure, Cc, is the isostructural with the Sr-IV structure. The calculation of the Cc

structure is performed at 50 K. The enthalpy calculation of the Cc structure is found that it decreases rapidly at the beginning (1 ps). Moreover, the Cc structure is shown that it is thermodynamically stable from 1.5 to 5 ps. The calculation of Cc suggests that the enthalpy of Cc is also thermodynamically favorable than the sc structure (see Fig. 11).

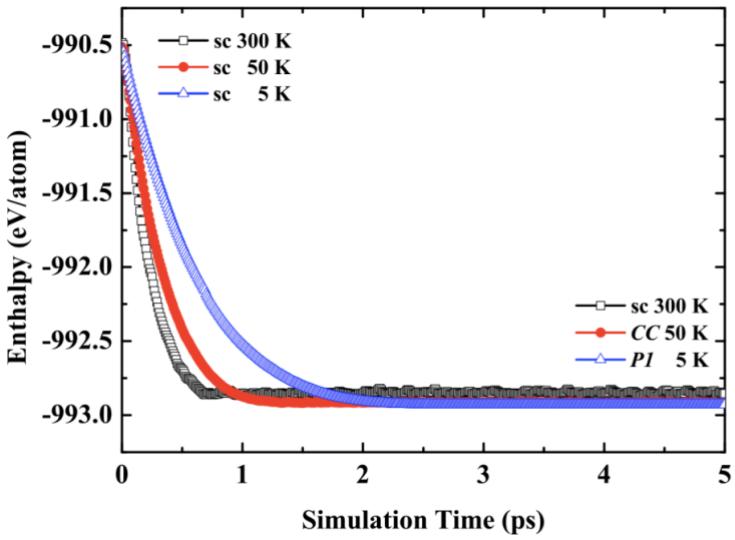

Figure 11. Simple-cubic (sc) supercells structure was calculated using MD simulation resulting in the appearance of the monoclinic complex superstructure, with space group Cc structure at a few picoseconds after the simulation has started. These graphs suggest that Cc is more stable than sc.

A powerful tool for predicting the crystal structures of Ca is the AIRSS technique and the USPEX method. They confirm that Cc structure is thermodynamically stable. In Fig.12, the crossing points of curves from each structure represent the structural transformation; the fcc structure transforms into the bcc structure at pressure 8 GPa, and then into the β-tin structure at pressure 32 GPa. The transition sequence totally agrees with previous theoretical and experimental studies reported by Yao *et. al*. [30] and Li *et al.* [81] At the higher pressure, in this research, The β-tin transforms into the Sr-IV type (Cc) structure at 75 GPa and then into host-guest structure at 202 GPa. It should be noted that the Cc structure of Ca is the similar structure to the Sr-IV which the Wyckoff position is 4a as shown Fig. 13.

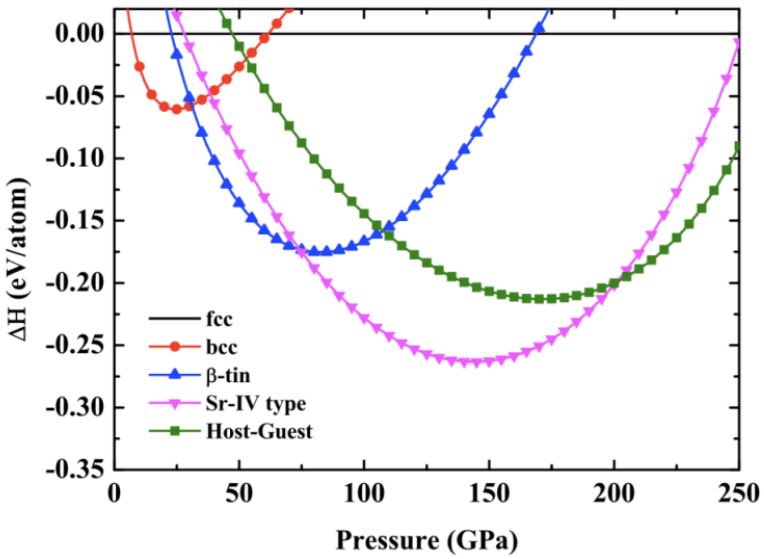

Figure 12. The enthalpy difference of bcc, β-tin, Sr-IV type, and host-guest structure related to the fcc structure at ambient pressure. The cross-section point of each line represents the occurring of transition event. The graph suggests that the transition will go from fcc ⟶ bcc ⟶ β-tin ⟶ Sr-IV type ⟶ host-guest, respectively.

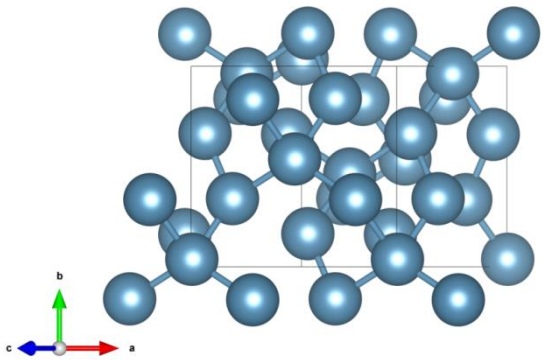

Figure 13. Structural optimization of Cc are a = 6.08050 Å, b= 5.93290 Å, c= 4.60520 Å, β=135.075° with Ca atom located 4a symmetry sites Ca1 [0.890313, 0.334935, 0.168998], Ca2 [0.611264, 0.160219, 0.332086], Ca3 [0.502043, 0.462576, 0.497116] at pressure160 GPa.

4.4 Structurre prediction of scandium at high pressure

In the ongoing strong efforts to provide the experimental and theoretical studies, [32-34] The Sc-II structure is expected to be the HG structure. However, the structure of Sc-II is not fully understood, especially the existence of two parameters, the c_H/c_G of the HG structure, at pressures 23 and 72 GPa. In this work, the calculation of the HG structure is concentrated by considering the relationship between the host and guest structures under high pressure. The host ($3c_H$), the guest ($4c_G$), and the c_H/c_G (4/3) of HG structures are calculated independently.

The first evidence for explaining the existence of the ideal c_H/c_G (4/3) of the HG structure is in good agreement with the experimental result [32] as can be seen Fig.14 Furthermore, the dynamical stability of the $3c_H$ structure, the $4c_G$ structure, and the c_H/c_G (4/3) of HG structures are confirmed by phonon dispersion calculations. Moreover, the calculation of the c_H/c_G (4/3) shows that the $3c_H$ structure and $4c_G$ structure have imaginary frequencies which indicate their unstable separate structures at pressure 70 GPa. However, the combined HG (4/3) structure is stable because of the absence of any imaginary frequencies as can be seen Fig. 14. It is

worth noting here that the HG structure is also stable with the ideal c_H/c_G parameter of 4/3.

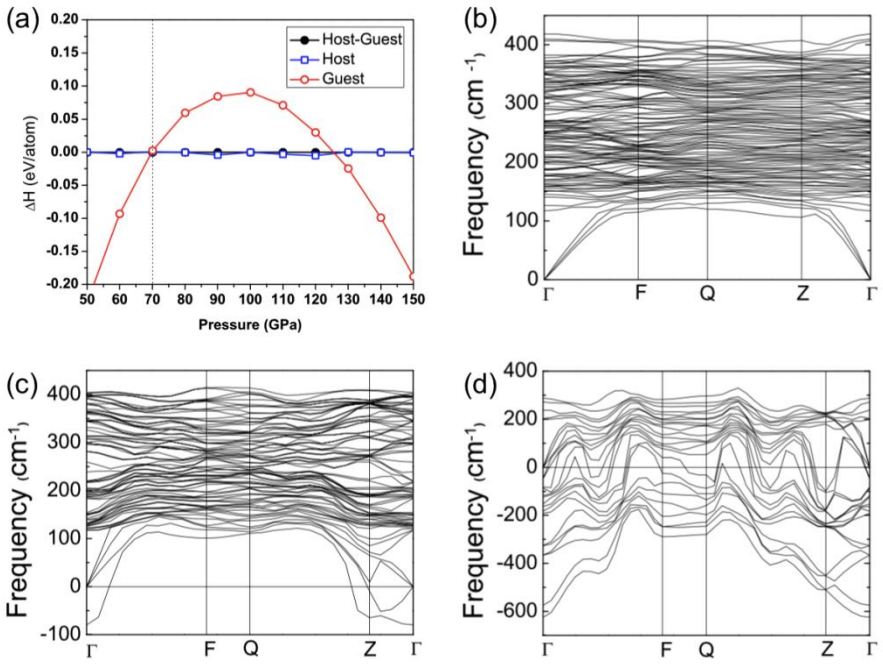

Figure 14. (a) The calculation is combined with the host and guest structures to become the host-guest structure. The calculated in this structure are examined by the enthalpy-pressure relation. The phonon calculation in the HG structure at pressure 70 GPa, with the commensurate value of 4/3. (b) The host-guest structure with the absence of any imaginary frequency. (c) The host structure is shown in the unstable structure. (d) The guest is also shown in the unstable structure.

In order to accurately calculate the existence of the commensurate value of 4/3, it is determined by the AIMD method. With the increasing temperature and pressure, the calculation of the commensurate value of 4/3 elucidates that it is stable at temperature 300 K and pressure 72 GPa. Moreover, the enthalpy of Sc-II (4/3) is found that it decreases rapidly from 0 to 0.25 ps. Furthermore, the enthalpy of Sc-II (4/3) is stable from 0.25 to 2 ps. This result can be seen in Fig. 15.

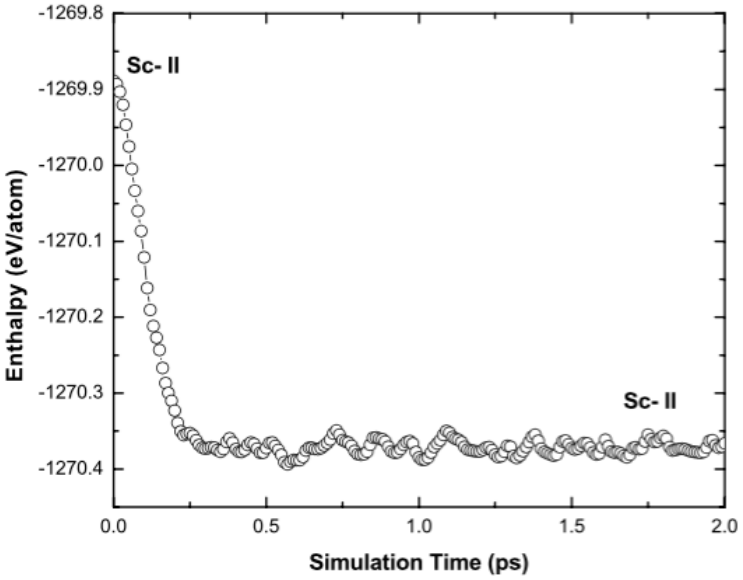

Figure 15. The calculated enthalpy (eV/atom) versus simulation time (ps) in Sc-II by performing the MD calculation at pressure 72 GPa and temperature 300 K. The calculated Sc-II is thermodynamically stable.

The transition sequence of Sc is successfully observed by the theoretical study and the experimental study [32-34]. Sc-I (hcp) transforms into Sc-II (HG) and then into the Sc-III. Unfortunately, the previous reports [32-34] show that the Sc-III structure is not fully understood. In order to identify the Sc-III (unknown) structure, the AIRSS technique has been used. This calculation leads to three probable spacegroups (Cmcm, $P2_1/c$, and $P4_12_12$). They are determined by the enthalpy-pressure relation with respect to the Sc-II structure.

The calculation indicates that the $P4_12_12$ structure is thermodynamically more favorable (see Fig. 16a). The optimized structural parameters of $P4_12_12$ structure are a = 4.12974 Å and c = 2.59857 Å with Sc atoms located at 4a symmetry site (0.701, 0.298, 0.25). The dynamic stability of the $P4_12_12$ structure is confirmed that it is stable at 120 GPa. The calculation elucidates that the phonon dispersion is the absence of any imaginary frequencies as shown in Fig. 16b. For pressure-induced structural phase transition, the Sc-II (c_H/c_G=4/3) structure transforms into the Sc-III ($P4_12_12$) structure. This remarkable result indicates that the transition sequence of pressure-induced phase transitions is from the hcp to HG at 32 GPa and then into the $P4_12_12$ at 93 GPa as can be seen in Fig. 17.

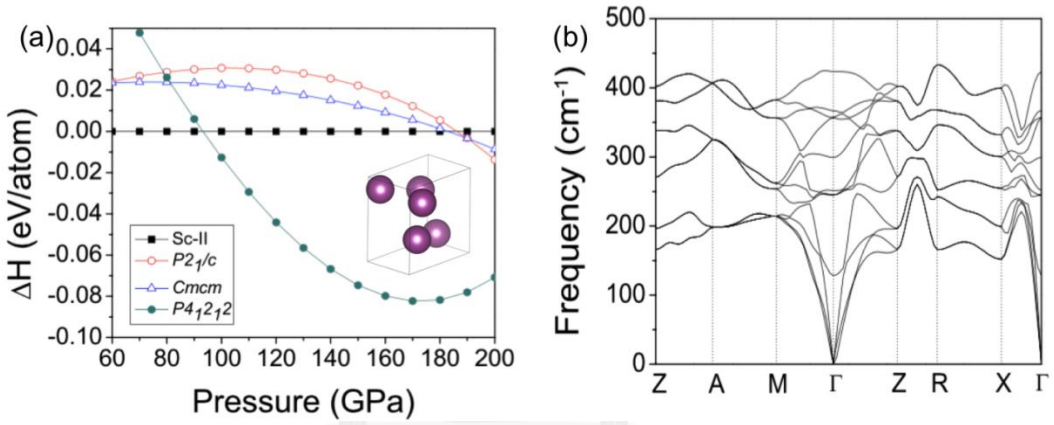

Figure 16. (a) The AIRSS calculations are presented in the enthalpy difference of $P2_1/c$, Cmcm, and $P4_12_12$ structures with respect to the Sc-II structure at high pressure. Sc undergoes a sequence of structural phase transitions with the increasing pressure, from Sc-II to $P4_12_12$. (b) The phonon dispersions of $P4_12_12$ structures at 120 GPa.

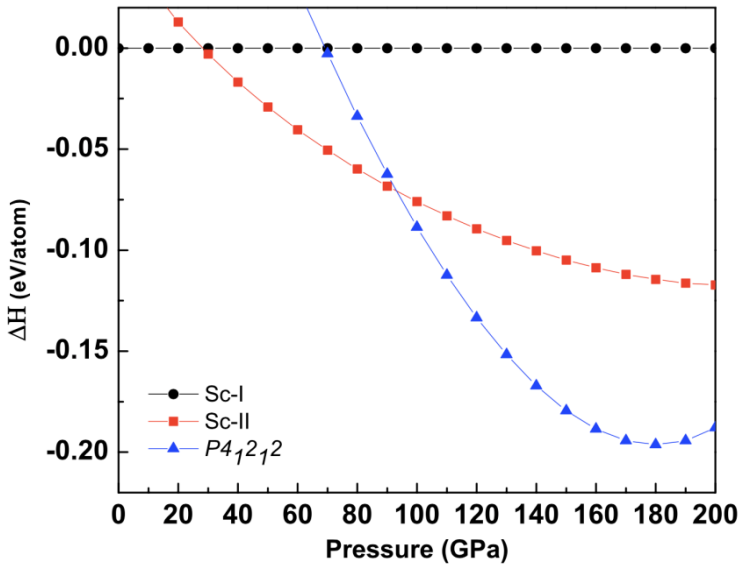

Figure 17. The enthalpy difference of the Sc-II and $P4_12_12$ structures with respect to the Sc-I structure at ambient pressure. The cross section point of each line represents the transition event. Sc undergoes a sequence of structural phase transitions with the increasing pressure, from Sc-I⟶ Sc-II⟶ $P4_12_12$.

4.5 Phase transition sequences of arsenic

The calculation of structure searching in As is performed above 100 GPa. The result finds that the lowest enthalpy structure of As is the body-centered tetragonal (bct) structure with spacegroup $I4_1/acd$. The simulated crystal structure of the bct structure is shown in Fig. 18 as implemented in VESTA [82]. The optimized structural parameters for the bct structure are a = 4.072 Å and c = 5.802 Å with As atoms located at 8a symmetry site (0, 0.5, 0.25).

With the increasing pressure, the transition sequence is successfully observed by the experimental study [37]. The sc structure of As transforms into the monoclinic host-guest (HG) structure at 48 GPa, and then into the body-centered cubic (bcc) structure at 97 GPa. On the contrary, this calculation proposes that transition sequence should be from the sc structure to the HG structure at 41 GPa and then to the bct structure at 81 GPa. Interestingly, the bcc structure is the supergroup (Im-3m) and the bct structure is subgroup ($I4_1/acd$) of the ordinary bcc structure. These two

structures are possible to coexist. The enthalpy calculation reveals that both enthalpy of the bcc and bct structures are remarkably close at the pressure range from 100 to 300 GPa.

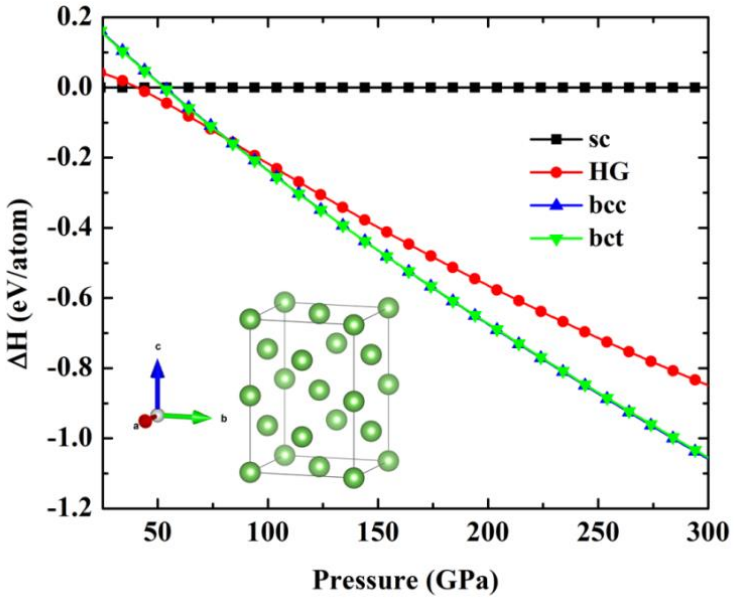

Figure 18. Comparison of the enthalpies of As phases up to 300 GPa.

In fact, the bcc and bct structures have very similar crystal structures. In order to determine the difference between the bcc and bct structures, Fig. 19 shows the simulated powder diffraction patterns at 100 GPa of the bcc and bct structures. The peak (200), (211), (220), and (310) of the bct structure are distorted from the bcc structure. The bct structure has been confirmed with slightly distorted parameter a/c lowered by 1% with respect to the bcc structure.

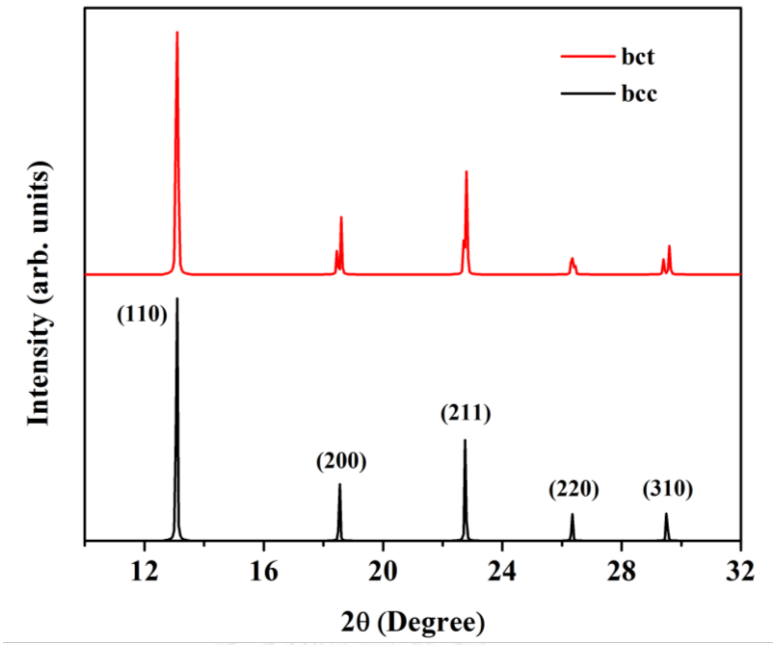

Figure 19. Simulated x-ray powder diffraction patterns of the bcc structure (black) and the bct structure (red).

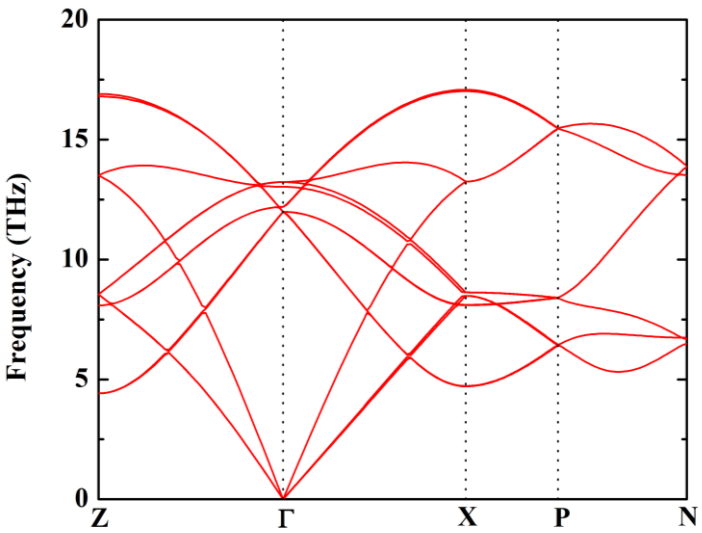

Figure 20. The dynamical harmonic stabilization of the bct structure at pressure 300 GPa.

This finding leads to a new stable structure of As at high pressure. Moreover, the dynamic stability of the bct structure is confirmed by phonon calculation. The lack of imaginary frequencies provides a clear confirmation that the bct structure is the most stable structure at 300 GPa (Fig. 20).

CHAPTER V
SUPERCONDUCTING TRANSITION TEMPERATURE

In this chapter, properties of Mg, Ca, Sc, and As under high pressure are presented and discussed especially for their superconducting transition temperature. For Mg, the high pressure normal metallic phase is predicted to be at the pressure above 160 GPa. For Ca, The calculation of the Cc structure is predicted with T_c of 25.2 K and at 160 GPa. For Sc, The AIRSS technique reveals the stable structure of Sc-III. The calculation of the Sc-III shows that superconductivity arises in the tetragonal $P4_12_12$ structure. For As, metallization of the bct structure is predicted to give a superconducting transition temperature of 4.2 K at 150 GPa. These calculated superconducting transition temperature of metals gives a clear understanding of the interpretation of elemental metal under extreme conditions.

5.1 Normal metallic structure of magnesium at high pressure

The calculation λ and ω_{log} as a function of pressure in both I4/mmm and Pnma structures at 160 and 250 GPa have been performed with the effective Coulomb interaction parameter μ^*= 0.10, which is assumed for all metals by Allen and Dynes [49] This result shows Eliashberg phonon spectral function evolution ($\alpha^2F(\omega)$), the phonon density of states (PhDOS) and the integrated λ as a function of pressure at 160 and 250 GPa for the I4/mmm and Pnma structures respectively (see Fig.21). By considering the behavior of λ under high pressure, it can be understood from the integral of spectral function up to any frequencies ω. At 160 GPa, For I4/mmm structure, it is found that the integrated λ is increased because of the phonon frequencies increase. Moreover, in Pnma structure, it is also is found that the integrated λ is also increased because of the phonon frequencies increase at 250 GPa. The obtained PhDOS of the I4/mmm and Pnma structures show the lack of imaginary frequencies as well as the electron-phonon coupling (EPC). In addition, the $\alpha^2F(\omega)$ of both structures is found to be lower than 5 THz with the increasing λ.

Moreover, it is contributed to lower frequencies more significant than over 5 THz (see Fig 21). However, the I4/mmm and Pnma structures show that the Eliashberg phonon spectral function is nearly zero. This remarkable result put the I4/mmm and Pnma structures to be common high-pressure structures which possess the normal metallic property similar to those of metal hydrides previously reported in YH_3 [83, 84], ScH_3[84], and LaH_3 [84].

By finding the normal metallic state at high pressure among AEM, Mg possesses the normal metallic property and it can also be considered through the Eliashberg phonon spectral function as a function of pressure. At 160 GPa the I4/mmm structure find the integrated λ is increased as the phonon frequencies increase. Likewise, at 250 GPa the Pnma structure also exhibit the similar trend. The I4/mmm indicated that the EPC increases (averaged phonon frequency ω_{log} decreases) between 160 and 200 GPa as can be seen in Fig. 22. At the pressure above 200 GPa, the Pnma indicates that the EPC also is increased monotonically (averaged phonon frequency ω_{log} decreases) between 250 and 400 GPa. It is worth noting that the EPC is rapidly decreased then it is substantially increased at the pressure above 200 GPa.

The c/a ratio of each structure is presented as a function of pressure. It is slightly increased from 160 to 200 GPa and then it is rapidly decreased due to it transforms into the Pnma structure. At the pressure above 221 GPa, the c/a ratio of the Pnma structure is slightly decreased with increasing pressure from 250 to 400 GPa, which is shown in Fig. 22.

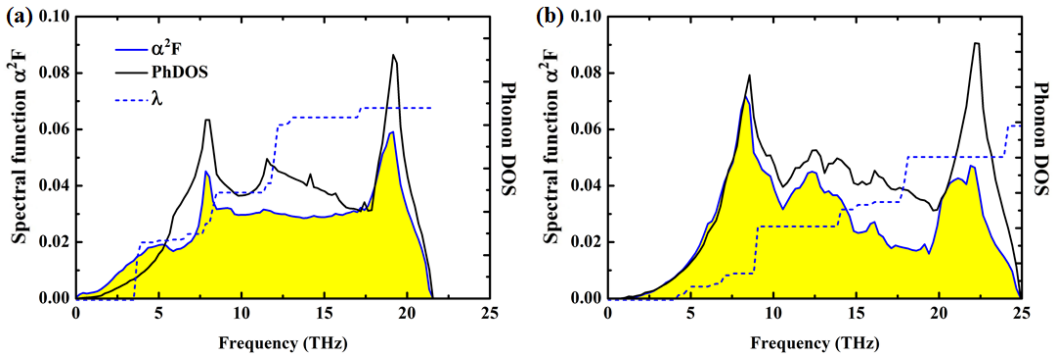

Figure 21. Spectral function $\alpha^2F(\omega)$ (blue line) and integrated λ (shot dash blue line) as a function of frequency at two different pressure values, namely, (a) I4/mmm at 160 GPa and (b) Pnma at 250 GPa, respectively.

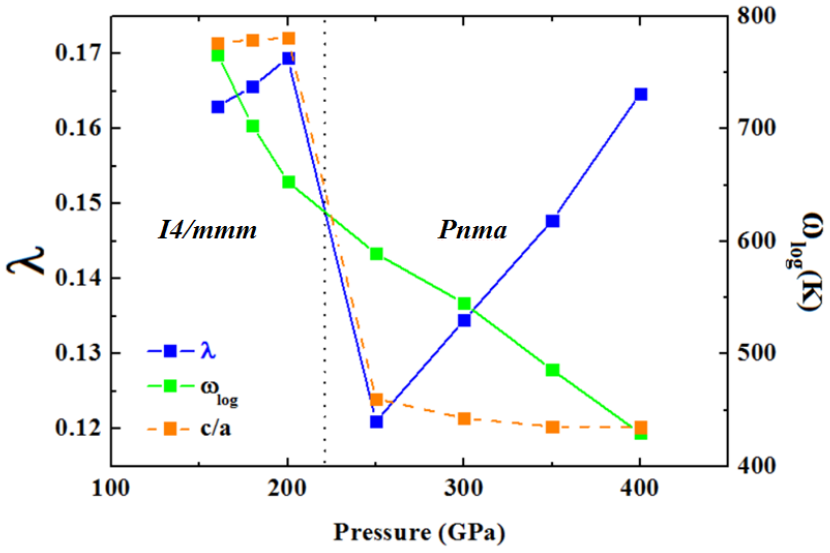

Figure 22. Our calculation show electron-phonon coupling (blue line) and the averaged phonon frequency ω_{log} (green line) as a function of pressure using effective Coulomb interaction parameter μ*= 0.10. The c/a ratio as a function of pressure (orange line).

Moreover, the calculation presents that the I4/mmm and Pnma structures are not superconducting because T_c is zero at pressures 160, 180, 200, 250, 300, 350, and 400 GPa. This result suggests that both I4/mmm and Pnma structures in Mg are normal metallic structures.

5.2 Superconducting transition temperature of the Cc structure in magnesium

The metallic of Cc structure is determined by densities of states (DOS) and projected densities of states (PDOS) with s, p, and d orbitals at pressure 160 GPa (see Fig.16.) In the Cc structure, PDOS is dominated by d-orbital near Fermi level. This result suggests that it is the metallic state [85]. For a striking feature of d-orbital, it is a steep band which leads to the discovery of the strong coupling and the high-T_c superconductivity.

The dynamical stability of the Cc structure is examined by phonon dispersion calculation. The absence of imaginary frequency at 160 GPa implies that the Cc structure is stable at 160 GPa (see Fig.24).

The T_c of Cc structure is determined by the electron-phonon coupling (λ), the averaged phonon frequency (ω_{log}), and effective Coulomb interaction (μ^*). Effective Coulomb interaction, μ^*, is a free parameter which is depend on metal type, e.g., $\mu^* = 0.13$ is suggested to be used for T_c calculation of transition metals [48], and $\mu^* = 0.10$ is used for ordinary metals [49]. Moreover, variation of μ^* values is found to satisfy computational and experimental results, e.g., $\mu^* = 0.10$ for bcc and Cmcm structure in Sr [69], $\mu^* = 0.15$ for fcc structure in Y [79], $\mu^* = 0.16$ for bcc structure in H_3S [71] and $\mu^* = 0.18$ for fcc structure in Y at low pressure [79].

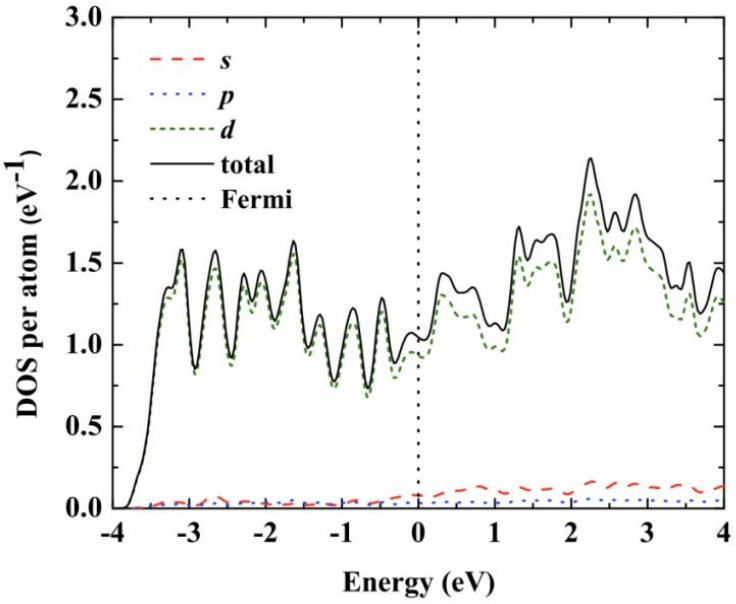

Figure 23. Total DOS, and projected DOS to s, p, and d orbitals of the Cc structure near the Fermi level at 160 GPa.

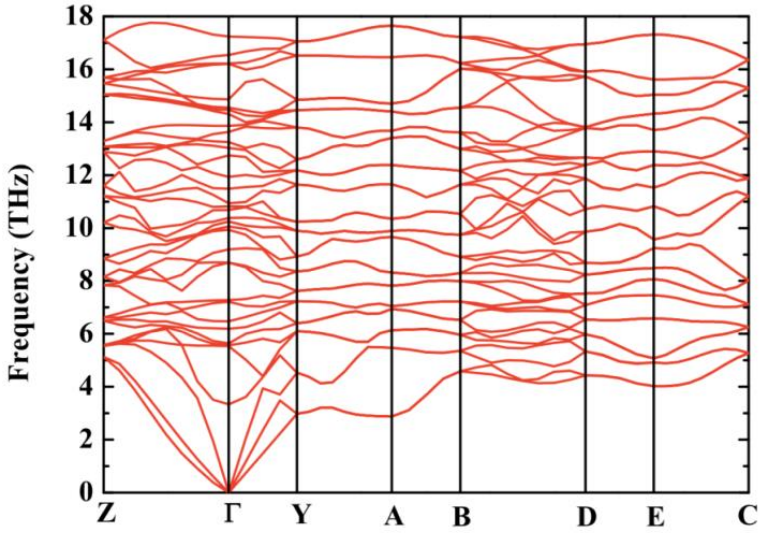

Figure 24. Phonon dispersion of the Cc structure is indicated the Kohn anomalies at pressure 160GPa. The phonon softening shows in branch along the Y⟶ A and A⟶ B directions.

The T_c of elemental metals mentioned above agreed with both computational and experimental studies by Allen-Dynes equation. Generally, the T_c is fitted from a designated μ* by Allen-Dynes equation. It is widely accepted to have λ less than 1.4.

In order to determine T_c of Ca, μ* is primarily designated to be 0.10, 0.13, 0.15, 0.16 0.18. And the Cc structure is used to fit for T_c at pressures from 120 to 160 GPa by Allen-Dynes equation. This calculation result puts the Cc structure to be the metallic state. The Cc structure is reported to possess the highest T_c with the T_c of 25.2 K at 160 GPa which is in good agreement with the reported value of 25 K at 161 GPa by Yabuuchi *et al.* [23].

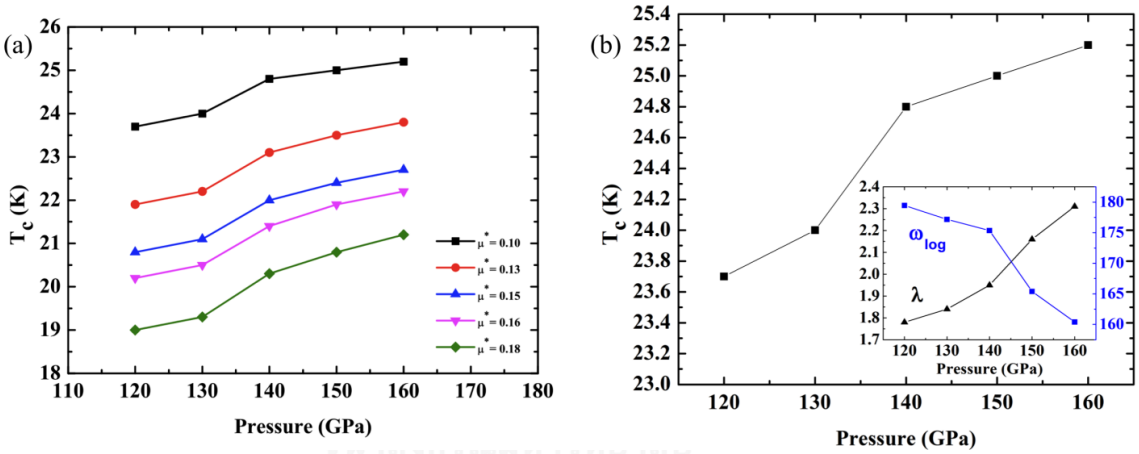

Figure 25. (a) Our calculated T_c vs pressure for Ca using five effective Coulomb parameters. (b) The effective Coulomb μ^*=0.10 shows the highest T_c and the inset shows calculated electron-phonon coupling (λ) and logarithmic phonon momentum (ω_{log}) as a function of pressure.

Because the Cc structure is the most stable structure in the pressure range 120-160 GPa. The phonon of the Cc structure reveals significant electron-phonon coupling. With the increasing pressure, the λ of Cc is increased (see Fig.25). Interestingly, the Cc structure finds that it is a strong electron-phonon coupling due to $\lambda > 2$ [79, 86] at above 140 GPa.

5.3 Superconducting transition temperature of Sc-III

Sc-II has been reported to be a superconductor [38]. The T_c has been measured up to 19.6 K at 107 GPa. [35] The second transition from the Sc-II phase to the Sc-III phase, it is also proposed to maintain its superconductivity with the T_c rapidly decreased to 8.31 K at 111 GPa. [11] Interestingly, it is worth noting that Hamlin *et al.* [38] does not observe a T_c at the pressure above 130 GPa. In this study, the T_c of Sc-III is explored in the $P4_12_12$ structure at pressures 110, 120, 130, and 140 GPa. The calculation finds that μ^*=0.13 is in good agreement with the experimental report as can be seen in Fig. 26a. The calculation shows that μ^*=0.13 [48] is given a better fit to experiment at 110 GPa. Besides, the T_c decreases monotonically between 110 and 150 GPa and the electron-phonon coupling also decreases with the increasing pressure although μ^*=0.10 [49] gives the highest T_c among other parameters.

The result of Sc is shown that it is in good agreement with the experimental study [35]. The T_c of the $P4_12_12$ structure is predicted by Allen-Dynes equation to be superconducting with the T_c of 8.36 K at 110 GPa. Moreover, the T_c of $P4_12_12$ structure slightly decreases with the increasing pressure. The average phonon frequency ω_{log} and the λ decrease monotonically between 110 and 140 GPa. The T_c of $P4_12_12$ structure is also decreased with the pressure as can be seen in the inset Fig. 26b. The phonon frequency increases with pressure above 100 GPa, but λ decreases with pressure, and T_c gradually declines with pressure as shown in Fig. 26b.

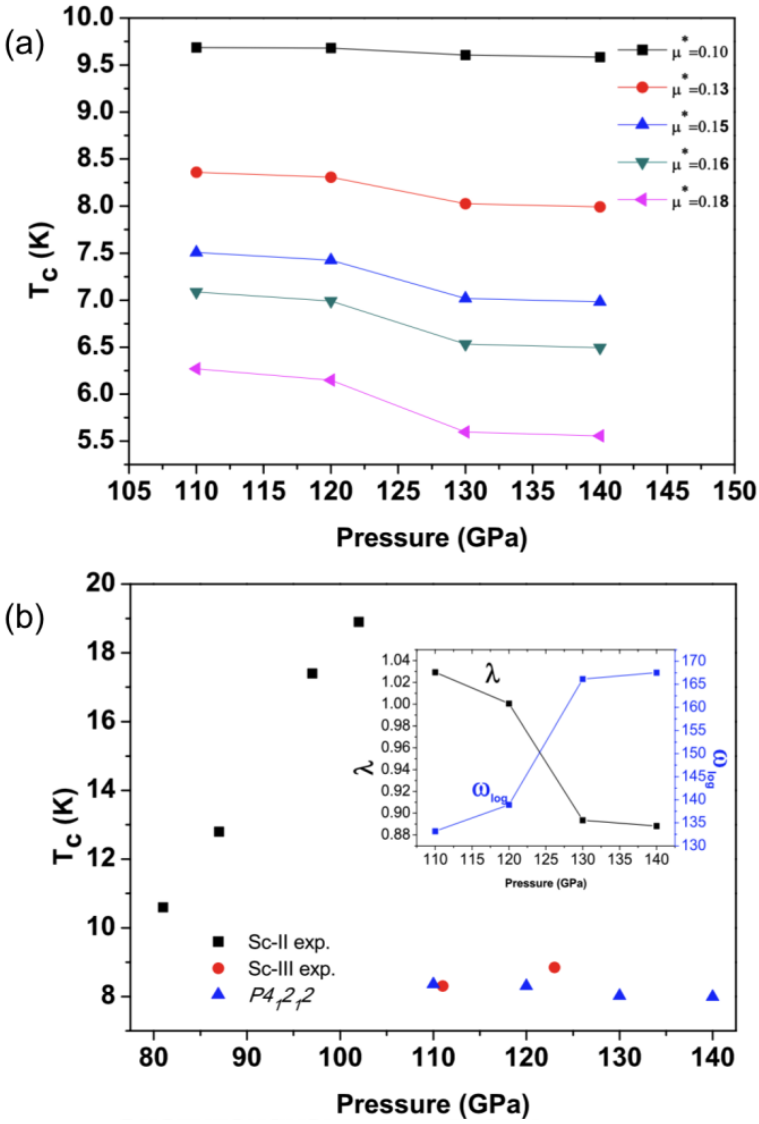

Figure 26. (a) Superconducting T_c of Sc as the function of pressure. The inset shows that values of ω_{log} and λ calculated for $P4_12_12$ structure. The solid symbols represent calculation and experimental literature [35] for the $P4_12_12$ (blue circles) the Sc-II (black circles) and Sc-III (red triangles) phases, respectively. (b) The several effective Coulomb interaction parameters are used to examine the T_c.

5.4 Spectral function of the bct and bcc structures in arsenic

At 150 GPa, the spectral function α^2F of bct arsenic is higher than those of the bcc structure around frequency region 6-13 THz. Likewise, the integrated λ of the bct structure is also higher than the bcc structure and it exhibits a metallization in the bct structure and it is predicted to give T_c of 4.2 K at 150 GPa as can be seen Fig.27.

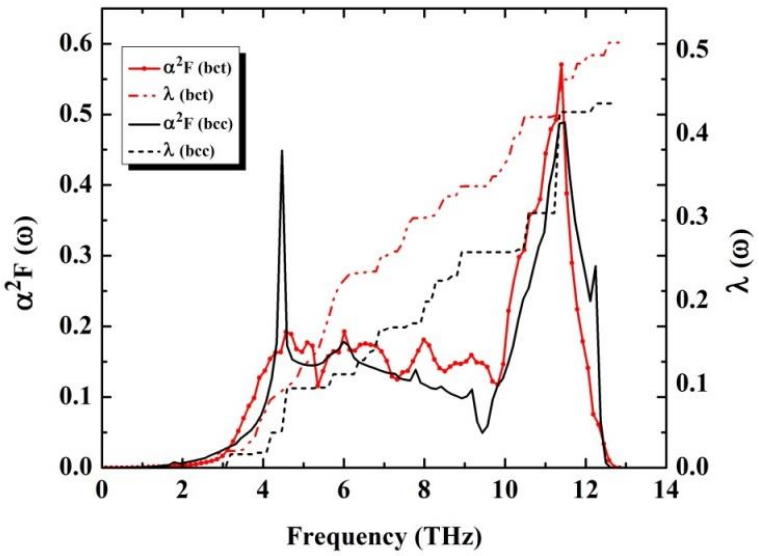

Figure 27. Spectral function $\alpha^2F(\omega)$ and integrated λ as a function of frequency of As at pressure 150 GPa.

The calculation reveals T_c between the bcc and bct structures with the increasing pressure which generally shows monotonic decreasing behaviors (see Fig.28). The λ of the bct structure is higher than the bcc structure at 150 GPa which leads to possibility of the highest T_c of As. It indicates that T_c of the bct structure is higher than the bcc structure. The bct possesses the highest T_c of around 4.2 K.

Above 150 GPa, the T_c of the bct structure is lower than the bcc structure as well as T_c gradually decreases with pressure. The λ of the bcc and bct structures decrease monotonically between150 GPa and 300 GPa respectively. The ω_{log} of the

bcc and bct structures increase between 150 GPa and 300 GPa respectively as can be seen the inset in Fig. 28.

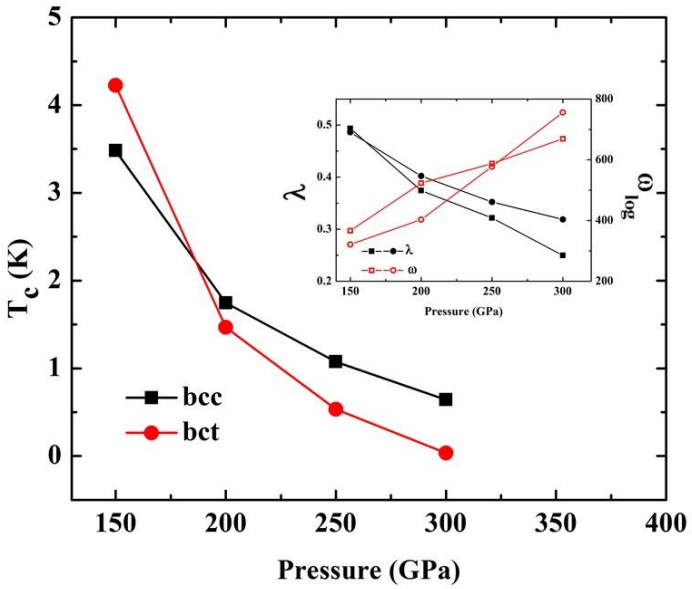

Figure 28. Superconducting T_c of As as a function of pressure. The square and the circle symbols represent calculations for the bcc and bct structures, respectively. The inset shows calculated electron-phonon coupling for the bcc structure (filled circle) and the bct structure (filled square) and averaged phonon frequency as a function of pressure for the bcc structure (hollow circle) and the bct structure (hollow square).

Moreover, this remarkable result strongly suggests that the bct structure is not possessed superconducting property above 300 GPa. This is due to the fact that the bct structure remains in the metallic state at 300 GPa, The calculation proposes that it is become a normal metallic state with the increasing pressure.

CHAPTER VI
CONCLUSION

In summary, new structures of Mg are predicted by the AIRSS method. It finds that the I4/mmm and the Pnma structures are thermodynamically stable at 0 K. This result shows that structural phase transformation sequence of Mg is from the ambient hcp structure to the bcc structure at 58 GPa and to the I4/mmm structure at 154 GPa and then into Pnma at 221 GPa. The phonon dispersion relation shows that the I4/mmm and Pnma structures are thermodynamically stable at pressures 160 and 250 GPa respectively. In addition, it suggests that the I4/mmm and the Pnma structures are normal metallic.

Moreover, the AIRSS calculation reveals a new stable HG structure in Li above 110 GPa. The calculation predicts the complex structural phase transformations at finite temperature and high pressure that the HG structure is stable above 110 GPa. It should be noted that the fcc structure can also generate the HG structure at the finite temperature and high pressure. The dynamical harmonic stabilization shows that it is stable at 180 GPa. The distribution of electrons between the host-host atoms is strongly localized electron of π bond which leads to the stability of this remarkable HG structure. This result confirms that Li can form the HG structure under high pressure and high temperature which puts the HG structure to be a common high-pressure structure among all alkali metals.

For Ca, the stability of sc structure is confirmed by AIMD calculation at room temperature. The sc structure transforms into the monoclinic structure with spacegroup Cc (Sr-IV type) at 60 GPa and 50 K. The DFT calculation reveals that pressure-induced phase transitions are from fcc to bcc and to β-tin and then to the Sr-IV type (Cc) and finally to the host-guest structure. It is similarly corresponded to the transition sequence of Sr. The calculated T_c of this predicted Cc structure is in an extremely good agreement with that of the experimental result. The Cc structure should also be worth examining experimentally at low temperature (30-50 K) and pressure between 120-160 GPa.

Furthermore, The Sc-II structure is identified with the c_H/c_G parameter of 4/3 at 70 GPa. The result is in excellent agreement with the experimental report. For the coexistence of the host structure and guest structure, it can lead to the whole new interpretation for the existence of HG structure in elemental metals. The calculation has shown that Sc undergoes a sequence of structural phase transitions with the increasing pressure, from Sc-I to Sc-II to $P4_12_12$ at pressure 32 and 93 GPa respectively. This is the first evidence for revealing a novel phase; Sc does not exhibit the common series of structural phase transformations observed in the trivalent rare-earth element. The $P4_12_12$ structure is predicted to be a superconducting phase with the T_c of 8.36 K which is in good agreement with the previous experimental report.

Finally, the AIRSS method reveals a new stable of As that is the bct structure with spacegroup $I4_1/acd$ at high pressure. The calculation shows that structural phase transformation of As from sc to HG and then to bct at 41, and 81 GPa respectively. The bct structure is thermodynamically stable above 81 GPa. The result shows that the bct structure is also dynamically stable at 300 GPa. Therefore, this result suggests the transition sequence to be from the sc structure to the HG structure at 41 GPa and then into the bct structure at 81 GPa. The calculation finds that the T_c of the bct structure is maximum around 4.2 K at 150 GPa. It is worth noting that from our calculation,both bct and bcc structures share the remarkable similar enthalpy as well as their properties. Thus, both structures may be observed by experimental study at low temperature and high pressure.

REFERENCES

1. McMahon, M.I., *et al*., *Composite incommensurate K-III and a commensurate form: Study of a high-pressure phase of potassium.* Physical Review B, 2006. **74**(14): p. 140102.
2. McMahon, M.I., S. Rekhi, and R.J. Nelmes, *Pressure Dependent Incommensuration in Rb-IV.* Physical Review Letters, 2001. **87**(5): p. 055501.
3. Lundegaard, L.F., *et al*., *Single-crystal studies of incommensurate Na to 1.5 Mbar.* Physical Review B, 2009. **79**(6): p. 064105.
4. Matsuoka, T., *et al*., *Pressure-induced reentrant metallic phase in lithium.* Physical Review B, 2014. **89**(14): p. 144103.
5. Hanfland, M., *et al*., *New high-pressure phases of lithium.* Nature, 2000. **408**(6809): p. 174-178.
6. Marqués, M., *et al*., *Crystal Structures of Dense Lithium: A Metal-Semiconductor-Metal Transition.* Physical Review Letters, 2011. **106**(9): p. 095502.
7. Hanfland, M., *et al*., *Equation of state of lithium to 21GPa.* Solid State Communications, 1999. **112**(3): p. 123-127.
8. Guillaume, C.L., *et al*., *Cold melting and solid structures of dense lithium.* Nature Physics, 2011. **7**(3): p. 211-214.
9. Goncharov, A.F., *et al*., *Spectroscopic evidence for broken-symmetry transitions in dense lithium up to megabar pressures.* Physical Review B, 2005. **71**(18): p. 184114.
10. Ma, Y., A.R. Oganov, and Y. Xie, *High-pressure structures of lithium, potassium, and rubidium predicted by an ab initio evolutionary algorithm.* Physical Review B, 2008. **78**(1): p. 014102.
11. Yao, Y., J.S. Tse, and D.D. Klug, *Structures of Insulating Phases of Dense Lithium.* Physical Review Letters, 2009. **102**(11): p. 115503.
12. Pickard, C.J. and R.J. Needs, *Dense Low-Coordination Phases of Lithium.* Physical Review Letters, 2009. **102**(14): p. 146401.

13. Skriver, H.L., *Calculated Structural Phase Transitions in the Alkaline Earth Metals.* Physical Review Letters, 1982. **49**(24): p. 1768-1772.
14. Olijnyk, H. and W.B. Holzapfel, *High-pressure structural phase transition in Mg.* Physical Review B, 1985. **31**(7): p. 4682-4683.
15. Moriarty, J.A. and A.K. McMahan, *High-Pressure Structural Phase Transitions in Na, Mg, and Al.* Physical Review Letters, 1982. **48**(12): p. 809-812.
16. Li, P., *et al.*, *Crystal Structures and Exotic Behavior of Magnesium under Pressure.* The Journal of Physical Chemistry C, 2010. **114**(49): p. 21745-21749.
17. Sakata, M., *et al.*, *Superconducting state of Ca-VII below a critical temperature of 29 K at a pressure of 216 GPa.* Physical Review B, 2011. **83**(22): p. 220512.
18. Stinton, G.W., *et al.*, *Equation of state and high-pressure/high-temperature phase diagram of magnesium.* Physical Review B, 2014. **90**(13): p. 134105.
19. Vasvari, B., A.O.E. Animalu, and V. Heine, *Electronic Structure of Ca, Sr, and Ba under Pressure.* Physical Review, 1967. **154**(3): p. 535-539.
20. Skriver, H.L., *Crystal structure from one-electron theory.* Physical Review B, 1985. **31**(4): p. 1909-1923.
21. Mao, W.L., *et al.*, *Distortions and stabilization of simple-cubic calcium at high pressure and low temperature.* Proceedings of the National Academy of Sciences, 2010. **107**(22): p. 9965-9968.
22. Olijnyk, H. and W. Holzapfel, *Phase transitions in alkaline earth metals under pressure.* Physics Letters A, 1984. **100**(4): p. 191-194.
23. Yabuuchi, T., *et al.*, *New high-pressure phase of calcium.* Journal of the Physical Society of Japan, 2005. **74**(9): p. 2391-2392.
24. Nakamoto, Y., *et al.*, *Crystal structure and electrical property of calcium under very high pressure.* Journal of the Physical Society of Japan, 2007. **76**(Suppl. A): p. 25-26.
25. Ishikawa, T., *et al.*, *High-pressure phases of calcium: Prediction of phase VI and upper-pressure phases from first principles.* Physical Review B, 2010. **81**(9): p. 092104.

26. Nakamoto, Y., *et al.*, *Ca-VI: A high-pressure phase of calcium above 158 GPa.* Physical Review B, 2010. **81**(14): p. 140106.
27. Arapan, S., H.-k. Mao, and R. Ahuja, *Prediction of incommensurate crystal structure in Ca at high pressure.* Proceedings of the National Academy of Sciences, 2008. **105**(52): p. 20627-20630.
28. McMahon, M.I., O. Degtyareva, and R.J. Nelmes, *Ba-IV-Type Incommensurate Crystal Structure in Group-V Metals.* Physical Review Letters, 2000. **85**(23): p. 4896-4899.
29. McMahon, M.I., *et al.*, *Observation of the incommensurate barium-IV structure in strontium phase V.* Physical Review B, 2000. **61**(5): p. 3135-3138.
30. Yao, Y., et al., *Stability of simple cubic calcium at high pressure: A first-principles study.* Physical Review B, 2010. **82**(9): p. 094107.
31. Fujihisa, H., *et al.*, *Incommensurate composite crystal structure of scandium-II.* Physical Review B, 2005. **72**(13): p. 132103.
32. McMahon, M.I., *et al.*, *Different incommensurate composite crystal structure for Sc-II.* Physical Review B, 2006. **73**(13): p. 134102.
33. Arapan, S., N.V. Skorodumova, and R. Ahuja, *Determination of the Structural Parameters of an Incommensurate Phase from First Principles: The Case of Sc-II.* Physical Review Letters, 2009. **102**(8): p. 085701.
34. Akahama, Y., H. Fujihisa, and H. Kawamura, *New Helical Chain Structure for Scandium at 240 GPa.* Physical Review Letters, 2005. **94**(19): p. 195503.
35. Debessai, M., J.J. Hamlin, and J.S. Schilling, *Comparison of the pressure dependences of T_c in the trivalent d-electron superconductors Sc, Y, La, and Lu up to megabar pressures.* Physical Review B, 2008. **78**(6): p. 064519.
36. Häussermann, U., K. Söderberg, and R. Norrestam, *Comparative Study of the High-Pressure Behavior of As, Sb, and Bi.* Journal of the American Chemical Society, 2002. **124**(51): p. 15359-15367.
37. Degtyareva, O., M.I. McMahon, and R.J. Nelmes, *High-pressure structural studies of group-15 elements.* High Pressure Research, 2004. **24**(3): p. 319-356.
38. Hamlin, J.J. and J.S. Schilling, *Pressure-induced superconductivity in Sc to 74GPa* Physical Review B, 2007. **76**(1): p. 012505.

39. Chan, K.T., B.D. Malone, and M.L. Cohen, *Electron-phonon coupling and superconductivity in arsenic under pressure.* Physical Review B, 2012. **86**(9): p. 094515.
40. Pickard, C.J. and R.J. Needs, *High-Pressure Phases of Silane.* Physical Review Letters, 2006. **97**(4): p. 045504.
41. Hohenberg, P. and W. Kohn, *Inhomogeneous Electron Gas.* Physical Review, 1964. **136**(3B): p. B864-B871.
42. Kohn, W. and L.J. Sham, *Self-Consistent Equations Including Exchange and Correlation Effects.* Physical Review, 1965. **140**(4A): p. A1133-A1138.
43. Perdew, J.P. and A. Zunger, *Self-interaction correction to density-functional approximations for many-electron systems.* Physical Review B, 1981. **23**(10): p. 5048-5079.
44. Perdew, J.P., K. Burke, and M. Ernzerhof, *Generalized Gradient Approximation Made Simple.* Physical Review Letters, 1996. **77**(18): p. 3865-3868.
45. Feynman, R.P., *Forces in Molecules.* Physical Review, 1939. **56**(4): p. 340-343.
46. Car, R. and M. Parrinello, *Unified Approach for Molecular Dynamics and Density-Functional Theory.* Physical Review Letters, 1985. **55**(22): p. 2471-2474.
47. Clark Stewart, J., *et al*., *First principles methods using CASTEP*, in *Zeitschrift für Kristallographie - Crystalline Materials*. 2005. p. 567.
48. McMillan, W.L., *Transition Temperature of Strong-Coupled Superconductors.* Physical Review, 1968. **167**(2): p. 331-344.
49. Allen, P.B. and R.C. Dynes, *Transition temperature of strong-coupled superconductors reanalyzed.* Physical Review B, 1975. **12**(3): p. 905-922.
50. Chris, J.P. and R.J. Needs, *Ab initio random structure searching.* Journal of Physics: Condensed Matter, 2011. **23**(5): p. 053201.
51. Zurek, E. and W. Grochala, *Predicting crystal structures and properties of matter under extreme conditions via quantum mechanics: the pressure is on.* Physical Chemistry Chemical Physics, 2015. **17**(5): p. 2917-2934.

52. Pickard, C.J., M. Martinez-Canales, and R.J. Needs, *Density functional theory study of phase IV of solid hydrogen.* Physical Review B, 2012. **85**(21): p. 214114.

53. Pickard, C.J., M. Martinez-Canales, and R.J. Needs, *Decomposition and Terapascal Phases of Water Ice.* Physical Review Letters, 2013. **110**(24): p. 245701.

54. Pickard, C.J. and R. Needs, *Aluminium at terapascal pressures.* Nature materials, 2010. **9**(8): p. 624-627.

55. Pickard, C.J. and R.J. Needs, *High-Pressure Phases of Nitrogen.* Physical Review Letters, 2009. **102**(12): p. 125702.

56. Pickard, C.J. and R.J. Needs, *Metallization of aluminum hydride at high pressures: A first-principles study.* Physical Review B, 2007. **76**(14): p. 144114.

57. Schusteritsch, G. and C.J. Pickard, *Predicting interface structures: From $SrTiO_3$ to graphene.* Physical Review B, 2014. **90**(3): p. 035424.

58. Sun, J., *et al.*, *Stable All-Nitrogen Metallic Salt at Terapascal Pressures.* Physical Review Letters, 2013. **111**(17): p. 175502.

59. Sun, J., *et al.*, *Persistence and Eventual Demise of Oxygen Molecules at Terapascal Pressures.* Physical Review Letters, 2012. **108**(4): p. 045503.

60. Wang, X., *et al.*, *Cagelike Diamondoid Nitrogen at High Pressures.* Physical Review Letters, 2012. **109**(17): p. 175502.

61. Blöchl, P.E., *Projector augmented-wave method.* Physical Review B, 1994. **50**(24): p. 17953-17979.

62. Kresse, G. and J. Furthmüller, *Efficient iterative schemes for ab initio total-energy calculations using a plane-wave basis set.* Physical Review B, 1996. **54**(16): p. 11169-11186.

63. Togo, A. and I. Tanaka, *First principles phonon calculations in materials science.* Scripta Materialia, 2015. **108**: p. 1-5.

64. Baroni, S., *et al.*, *Phonons and related crystal properties from density-functional perturbation theory.* Reviews of Modern Physics, 2001. **73**(2): p. 515-562.

65. Paolo, G., *et al*., *QUANTUM ESPRESSO: a modular and open-source software project for quantum simulations of materials.* Journal of Physics: Condensed Matter, 2009. **21**(39): p. 395502.

66. Monserrat, B., *et al*., *Hexagonal structure of phase III of solid hydrogen.* Physical Review B, 2016. **94**(13): p. 134101.

67. Monserrat, B., et al., *Electron-Phonon Coupling and the Metallization of Solid Helium at Terapascal Pressures.* Physical Review Letters, 2014. **112**(5): p. 055504.

68. Martinez-Canales, M., C.J. Pickard, and R.J. Needs, *Thermodynamically Stable Phases of Carbon at Multiterapascal Pressures.* Physical Review Letters, 2012. **108**(4): p. 045704.

69. Kim, D.Y., *et al*., *Phase stability and superconductivity of strontium under pressure.* Applied Physics Letters, 2012. **101**(5): p. 052604.

70. Kim, D.Y., *et al.*, *Predicted Formation of Superconducting Platinum-Hydride Crystals under Pressure in the Presence of Molecular Hydrogen.* Physical Review Letters, 2011. **107**(11): p. 117002.

71. Errea, I., *et al*., *High-Pressure Hydrogen Sulfide from First Principles: A Strongly Anharmonic Phonon-Mediated Superconductor.* Physical Review Letters, 2015. **114**(15): p. 157004.

72. Srepusharawoot, P., *et al*., *One-dimensional polymeric carbon structure based on five-membered rings in alkaline earth metal dicarbides BeC_2 and MgC_2.* Physical Review B, 2010. **82**(12): p. 125439.

73. Nelmes, R.J., *et al*., *Self-Hosting Incommensurate Structure of Barium IV.* Physical Review Letters, 1999. **83**(20): p. 4081-4084.

74. Oganov, A.R. and C.W. Glass, *Crystal structure prediction using ab initio evolutionary techniques: Principles and applications.* The Journal of chemical physics, 2006. **124**(24): p. 244704.

75. Vanderbilt, D., *Soft self-consistent pseudopotentials in a generalized eigenvalue formalism.* Physical Review B, 1990. **41**(11): p. 7892-7895.

76. Monkhorst, H.J. and J.D. Pack, *Special points for Brillouin-zone integrations.* Physical Review B, 1976. **13**(12): p. 5188-5192.

77. Birch, F., *Finite Elastic Strain of Cubic Crystals.* Physical Review, 1947. **71**(11): p. 809-824.

78. Andersen, H.C., *Molecular dynamics simulations at constant pressure and/or temperature.* The Journal of chemical physics, 1980. **72**(4): p. 2384-2393.

79. Kim, D.Y. and R. Ahuja, *Ab initio study on pressure-induced change of effective Coulomb interaction in superconducting yttrium.* Applied Physics Letters, 2010. **96**(2): p. 022510.

80. Neaton, J.B. and N.W. Ashcroft, *Pairing in dense lithium.* Nature, 1999. **400**(6740): p. 141-144.

81. Li, B., *et al*., *Calcium with the β-tin structure at high pressure and low temperature.* Proceedings of the National Academy of Sciences, 2012. **109**(41): p. 16459-16462.

82. Momma, K. and F. Izumi, *VESTA 3 for three-dimensional visualization of crystal, volumetric and morphology data.* Journal of Applied Crystallography, 2011. **44**(6): p. 1272-1276.

83. Kim, D.Y., R.H. Scheicher, and R. Ahuja, *Predicted High-Temperature Superconducting State in the Hydrogen-Dense Transition-Metal Hydride YH_3 at 40 K and 17.7 GPa.* Physical Review Letters, 2009. **103**(7): p. 077002.

84. Kim, D.Y., *et al*., *General trend for pressurized superconducting hydrogen-dense materials.* Proceedings of the National Academy of Sciences, 2010. **107**(7): p. 2793-2796.

85. Ahuja, R., *et al*., *Theoretical Confirmation of the High Pressure Simple Cubic Phase in Calcium.* Physical Review Letters, 1995. **75**(19): p. 3473-3476.

86. Yin, Z.P., F. Gygi, and W.E. Pickett, *Competing phases, strong electron-phonon interaction, and superconductivity in elemental calcium under high pressure.* Physical Review B, 2009. **80**(18): p. 184515.

APPENDIX

APPENDIX A

Phase transition

The thermodynamic state of the elemental metals at equilibrium is explained by pressure, volume, temperature, entropy internal energy, and other thermodynamic potentials. The relation between thermodynamically stable, electronic structure allows us to compare the difference of the crystal structures. In this study, the calculation of the elemental metals has used the Kohn-Sham equation, as calculated at 0 K. By considering the stable structure, the calculation used the enthalpy:

$$H(P) = E(V) + PV,$$

where the pressure *P* is defined as

$$P(V) = -\left(\frac{\partial E(V)}{\partial V}\right)_T,$$

the calculation can examine the dependence of total energy of system on its volume $E = E(V)$ and to calculate the enthalpy as the pressure of pressure. The transition pressure $P_{1\to 2}$ from phase 1 to phase 2 can determine by the enthalpy. With increasing pressure, the stability of the crystal structure is the one which has the lowest enthalpy. In other words, the transition pressure $P_{1\to 2}$ is found from condition $H_1(P) = H_2(P)$ or $\Delta H(P) = 0$

Generally, the equilibrium unit cell parameter and the position of atoms in the unit cell must be examined by the optimization procedure at each volume.

APPENDIX B

Comparison of pseudopotentials

This thesis calculates the ground state energy by the CASTEP code and the VASP code. The calculation of metals uses two pseudopotentials. For the CASTEP code, the calculation uses ultrasoft pseudopotential. For the VASP code, the calculation uses projector augmented wave. Since the CASTEP code is not implemented projector augmented wave. The calculation for this research uses the AIRSS technique and the CASTEP code for prediction crystal structure. The result is shown that it is a good agreement with the CALYSO code and the VASP code (http://pubs.acs.org/doi/abs/10.1021/jp108136r). Thus, this thesis is referred to the following references

1. http://pubs.acs.org/doi/abs/10.1021/jp108136r

2. https://journals.aps.org/prl/abstract/10.1103/PhysRevLett.108.045503

3. https://journals.aps.org/prl/abstract/10.1103/PhysRevLett.116.025501

4. http://www.nature.com/nchem/journal/v6/n7/full/nchem.1925.html

5.http://iopscience.iop.org/article/10.1088/0953-8984/23/5/053201/meta;jsessionid=22C6FC762A84E543EE65124BF2C3F2D5.c2.iopscience.cld.iop.org

These references use the AIRSS technique, the CASTEP code, the CALYSO code and the VASP code to predict the crystal structure at high pressure.

VITA

Prutthipong Tsuppayakorn-aek was born in Pattani, Thailand on January 03, 1986. In 2009, he received a B.Sc. in Ed. degree in Physics from Prince of Songkla University, Pattani campus. In 2013, he received M.Sc. degree in Physics from Chulalongkorn University. Afterward, he started his Ph.D. study and work on his research at Extreme Condition Physics Research Laboratory, Chulalongkorn University since 2013. Ph.D. degree in Physics at Chulalongkorn University in 2016.

Publications

1. Tsuppayakorn-aek, P., Luo, W., Ahuja, R. and Bovornratanaraks, T. (2016) Stable normal metallic structure in Mg at high pressure. Scientific Reports (In press)

2. Tsuppayakorn-aek, P., Watcharatharapong, T., Luo, W., Ahuja, R. and Bovornratanaraks, T. (2016) Structural prediction of host-guest structure in lithium at high pressure. Physical Review Letters (In press)

3. Tsuppayakorn-aek, P., Luo, W., Ahuja, R. and Bovornratanaraks, T. (2016) The high-pressure superconducting phase of arsenic. Physical Review B (In submitted)

4. Tsuppayakorn-aek, P., Chuenkingkeaw, K., Kaewmaraya, T., Ahuja, R. and Bovornratanaraks, T. (2016) Stability of the commensurate value 4/3 of Sc-II and the pressure-induced superconductivity of Sc-III under high pressure (In manuscript)

5. Tsuppayakorn-aek, P., Chaimayo, W., Kotmool, K., Pinsook, U., Ahuja, R. and Bovornratanaraks, T. (2016) Predicted high-temperature superconducting phase of superstructure Sr-IV in calcium at high pressure (In manuscript)